Robotica (2022), **40**, pp. 1–37
doi:10.1017/S0263574721000357

CAMBRIDGE UNIVERSITY PRESS

RESEARCH ARTICLE

Design and control of a cable-driven rehabilitation robot for upper and lower limbs†

Efe Levent Oyman[1], Muhammed Yusuf Korkut[2], Cüneyt Yilmaz[1], Zeki Y. Bayraktaroglu[3] and M. Selcuk Arslan[1]*

[1]Yildiz Technical University, Department of Mechatronics Engineering, Istanbul, Turkey, [2]Istanbul Technical University, Graduate School of Science Engineering and Technology, Istanbul, Turkey and [3]Istanbul Technical University, Mechanical Engineering Department, Istanbul, Turkey
*Corresponding author. Email: msarslan@yildiz.edu.tr

Received: 24 September 2020; **Revised:** 11 March 2021; **Accepted:** 12 March 2021; **First published online:** 19 April 2021

Keywords: Rehabilitation robot, Impedance control, Therapeutic exercise, Cable-driven robot

Abstract

The design and control of a cable-driven rehabilitation robot, which can be configured easily for exercising different articulations such as elbows, shoulders, hips, knees and ankles without requiring any orthosis, are introduced. The passive, active-assisted and active-resisted exercises were designed and implemented using impedance control. The controller could switch between exercises according to the force feedback. The effectiveness of the proposed controller was demonstrated by experimental studies. The robot was tested first with a dummy extremity and then with a healthy subject mimicking various types of patients during the tests. Experimental results showed that satisfactory closed-loop performances were achieved.

1. Introduction

A physical rehabilitation aims to increase the functional abilities of the people who have physical disorders and to regain the motor functions they have lost [1]. The physical rehabilitation progresses are still widely performed by substantially applying forces to or moving the patient limbs and joints by physiotherapists. This situation has some disadvantages such as the physiotherapist's spending a long time and making too much effort, and the patient's being unable to follow the procedure because of the fatigue of the physiotherapist during the long exercise session.

The usage of the robotic products has significantly increased in the rehabilitation sector in recent years [2, 3, 4]. Rehabilitation procedures could be planned and applied more efficiently and practically, and the treatment could be followed with better understanding, and furthermore, the improvement could be seen in a shorter period of time by using these kinds of devices as an aid in the physiotherapy. At the current stage the rehabilitation robotics reached, it could be possible to assist various motor functions and to determine the motor performance of the patient [5, 6]. The use of robots in the physical rehabilitation applications decreases the workload of healthcare officers; hence, the cost of therapy procedures reduces [7]. On the other hand, a robot-aided rehabilitation improves the motor functions of patients better and faster compared to the conventional rehabilitation applications [8, 9].

Rehabilitation robots have been in the scope of many academic studies, and their importance has been more and more understood. They are classified into two groups with respect to their mechanical structures: (1) assistive robotic manipulators and (2) external skeleton (exoskeleton) robots. An assistive robotic manipulator which is mounted on a fixed place, such as a wall or a floor or a wheel chair or so,

†The online version of this article has been updated since original publication. A notice detailing the change has been published at https://doi.org/10.1017/S026357472300019X

is connected to a patient's limb via its end-effector, and it can apply forces only from the place where it is connected to the patient. The advantages of these devices are that they are simple, convenient and low cost and can be easily arranged for different extremity sizes. On the other hand, their disadvantages are that the posture of the extremity or the interaction torques of each joint cannot be accurately determined because the robot and the patient interact only at the end-effector of the robot. The most well-known robot for upper limb rehabilitation applications is MIT-MANUS robot, which is used for the treatment of the patients with stroke [10]. The studies with MIT-MANUS showed that the patients who had robotic therapies in addition to manual (conventional)ones recovered better and faster than the patients who had no robotic therapy [11].

An exoskeleton robot is attached to each joint of the patient's extremity and makes the patient exercised so as to comply with the movement of the extremity. The advantages of these types of robots are that they can exactly determine the posture of the extremity and they can individually control the torques applied to each joint. Their disadvantages are the need to adjust the robot segments according to the size of the extremity and the difficulty of attaching to the patient. One of the most known exoskeleton robots is ARMin, which was developed by Nef et al. [12, 13].

The rehabilitation robots can also be classified into three groups according to the exercise patterns: (1) passive, (2) active and (3) interactive rehabilitation robots. The passive rehabilitation robots are safer, lighter, cheaper and easier to use than other types of rehabilitation robots. The disadvantage of these robots is that they cannot aid the patient under the effect of a force other than the gravitational one. These types of robots are suitable for treatment of the paretic patients. The active rehabilitation robots are the devices that can control the interaction forces between the patient and itself or directly control the positions of the extremities. These types of robots, which can assist or resist the patient, are also used to precisely measure the active forces, range of motions and to determine spasticity levels of the patients [14, 15]. The interactive robots include sophisticated control methods, which can react according to the efforts of the patients. In these kinds of robots, the interaction is determined by feeding back the signals of position and force sensors to the controllers [16].

In the rehabilitation robots, various control approaches have been used such as proportional–integral–derivative (PID) position and force control, impedance control and adaptive control methods. The simplest and common one is the PID position control method, which is used for trajectory tracking for repeated passive exercises. Because it is neither a compliant nor flexible method, it is not effective at force-based applications such as active-assisted and strengthening exercises. To deal with this problem, it can be used together with adaptive and fuzzy control methods [17, 18]. Another control approach is hybrid position and force control one, which consists of an independent position and a force control loops at the same time. The rehabilitation devices with this control approach do not only move along the desired trajectory but also provides certain interaction forces [19]. In the impedance control method, the force feedback is received from the sensors to provide a position control, which complies with the patient's movement, rather than a classical position control [20]. Since the impedance-based controllers are flexible and compliant unlike the PID controllers, they are very appropriate and frequently used in the rehabilitation robots [21, 22]. Some researchers use electromyography (EMG) sensors to detect the muscle activities on the extremity of the patient, and the EMG signals are used as feedback data in the control system. The EMG-based control systems utilize EMG signals to estimate the joint angle for torque or provide continuous proportional torque assistance [19]. An adaptive control system has a capability of modifying its own parameters to achieve the best possible mode of operation. In other words, it continuously estimates the present state of the system to adapt its parameters for an optimal performance.

ROMRES (Range of Motion Rehabilitation System) is a novel patented neurological rehabilitation robot, which can make patients do exercises for both upper and lower limbs within a wide range of motion [23]. ROMRES can be categorized as a parallel end-effector-based cable-driven assistive rehabilitation device. As a mechatronic system, ROMRES was designed to serve for the largest number of exercise types. This robot can move any limb by driving the cables attached to the limb by means of pulleys

https://doi.org/10.1017/S0263574721000357 Published online by Cambridge University Press

connected to servo motors. As the limb rotates with respect to the support point, which is the bed in this system, the pulley mechanisms are translated vertically through elevators so that the cables are always perpendicular to the limb. As a system with both cables and elevators, it can be used for different limbs, as well as offering richness in exercise types. The types of exercises that can be done with ROMRES are shown in Fig. A1 given in Appendix.

Another optional feature of the robot is that it can do the exercises in the ways different from the known ones in the literature. Instead of intensive exercises of the patient's limb only on one side, it can be operated in the opposite direction at very short intervals (impulsive motion) allowing the muscles on the other side to work.

The robot can perform three main exercises: passive exercise, active-assisted exercise and exercise on spasticity. During a passive exercise, the extremity of the patient is moved according to the given position and velocity references. During the active-assisted exercise, the patient is allowed to freely move the extremity, while the system applies small amount of force (approximately 150 g) to compensate limb weight and frictions. In case of a spasticity exercise, the system changes the direction of the movement based on the reaction from the patient and moves the extremity in the direction of spasticity.

In order to perform the exercises, the behavior of the motors on both sides of the robot is controlled in the higher layer. It is a rule-based control system and determines the response of the device according to the patient's behavior. This layer consists of a state machine with five states for each direction of movement. In real time, these states switch the controllers, depending on the selected exercise type and the patient's behavior. PD controller for elevators and impedance controller for patient–robot interaction were designed. In order to cancel the effects of frictions and disturbances especially in the pulley system, a disturbance observer was designed. Hence, the system was able to operate with a high performance.

A motorized dummy arm was designed for initial tests to evaluate the overall performance of the system and to make improvements. Following successful tests, the system has been made ready to work with human subjects. In the last stage of this study, experiments were carried out for three different types of exercises with a healthy subject mimicking various types of patients. The tests for passive and active exercises were successfully performed. More remarkably, in the exercise on spasticity, when resistance is exerted by the subject against the movement applied by the robot, the robot was able to change the movement of the limb in the direction of the resistance to relax the patient. All experimental results have shown that the designed robot can successfully perform all exercises, maintaining the stability in the human–robot interaction.

The main contribution of this research to the literature is the design and control of a novel cable-driven rehabilitation robot, which can be configured easily for exercising different articulations such as elbows, shoulders, hips, knees and ankles. There are some variety of cable-driven rehabilitation robots in the literature [24, 25, 26, 27, 28, 29, 30, 31, 32, 33]. Among them, Alamdari et al. proposed a cable-driven rehabilitation robot called ROPES, which can be used for lower extremities [24] and Jin et al. proposed another cable-driven rehabilitation system for a gait training [25]. These devices made important contributions to the literature in the field of cable-driven rehabilitation. However, they need an exoskeletal orthosis to attach the patient's extremity and cannot be suitable for a rehabilitation procedure in the bed.

Cable-driven rehabilitation robots have several advantages such as simple architecture, low inertia, high load-to-weight ratio, modularity, no joint misalignment and suitability for reconfiguration [34]. Most of these robots are categorized as serial and parallel with subcategories of exoskeleton-based and end-effector-based. In ROMRES, the two cables are attached to the splint (end-effector) and the motorized reels. Thus, a large workspace without restricting the natural DOFs of the human limbs can be attained. By means of these two cables, any limb can be actuated bidirectional. The effect of weight of the limb on the cables is determined initially and taken into account by the software. Thanks to its adaptability feature, patients with various physical parameters, such as size and shape, can be accommodated. The elevator mechanism provides the motorized reel to be positioned vertically so that the applied force vector at the limb through the cables can be kept fixed as the limb rotates with respect to its joint.

https://doi.org/10.1017/S0263574721000357 Published online by Cambridge University Press

Table I. *Comparison of parallel end-effector-based cable-driven rehabilitation robots.*

Features/systems	**[36]**	**[37]**	**[38]**	**[39, 40]**	**[41]**	**[44]**	**ROMRES**
For upper limbs	○	○	○	○	○	×	○
For lower limbs	×	×	×	×	○	○	○
Adaptability	×	○	○	○	○	○	○
Versatility	×	×	×	×	○	○	○
Portability	○	○	×	○	×	×	○
Patient progress tracking	×	×	×	○	×	×	○
Impedance control feature	○	×	×	×	×	×	○
Range of motion allowed	M	M	M	M	H	H	H
Direction of actuation	B	B	U	U	U	B	B
Weight	M	M	M	H	M	H	M
Bulkiness	M	M	H	H	H	H	H

○ – available. × – unavailable. L/M/H – Low/Medium/High. U/B – Unidirectional/Bidirectional.

Having a large workspace together with bidirectional actuation ability makes ROMRES a highly versatile device. On the other hand, most of the parallel end-effector-based cable-driven rehabilitation robots are not portable; ROMRES is portable as it is designed compact and modular for both home and clinical usage. Additionally, the rehabilitation is both comfortable and simple, since the cable-driven mechanism is light and flexible. The special design of ROMRES allows binding to the patient with a single splint, which is simply a cuff, and doing an intensive treatment to the inpatients without any inconvenience for a long time. This structure not only provides a comfort to the patient but also allows the healthcare worker to easily bind the patient to the robot.

Although some parallel end-effector-based cable-driven rehabilitation devices are reported in the literature, many of them either are remained in the design stage or do not show experimental practice and results. Table I shows the available features of the referenced devices and ROMRES comparatively. In this comparison, only cable-driven real devices are included, whereas cable-driven exoskeletons and devices to rehabilitate the hands, fingers and gait are excluded for a fair comparison. For recent reviews on the cable-driven exoskeleton-based rehabilitation devices, the reader is referred to refs. [34, 35].

A planar desk-mounted cable-driven device for the passive rehabilitation of shoulders is reported in ref. [36]. The motion of the upper limb is measured by an optical tracking system to analyze the motion during the exercise. Although four different rehabilitation exercises are introduced, only results of passive exercise are shown. In ref. [37], another desk-mounted planar cable-driven rehabilitation device is introduced. Use of three cables and only one moving pulley block makes the system underactuated. To provide bidirectional actuation, optimal cable configuration is described analytically and the reconfiguration problem is solved. A cable-driven device that moves upper limbs translationally and unidirectional in 3D space is studied in ref. [38]. A sliding-mode controller was designed to control the motion of upper limbs under the effect of external disturbances. NeReBot [39] and MariBot [40] are cable-driven parallel robots designed for the rehabilitation of the upper limb of hemiplegic stroke survivors. Both robots have three cables to move the forearm of the patient. NeReBot has 3-DOF, and MariBot is a 5-DOF robot which is developed from NeReBot by addition of two serial linkages. A parallel end-effector-based cable-driven robot, which is similar to ROMRES in some ways, is reported in refs. [41, 42, 43]. It is not bidirectional, so it needs gravitational force for any return motion. Also, it lacks a mechanism to keep the applied force vector at the limb fixed. A novel design of a cable-driven lower limb rehabilitation robot with five rails is introduced in ref. [44]. According to the end-effector position on the leg, the actuators move along the rails to keep the tension on the cables constant. This function is similar to that of the elevator mechanism of ROMRES. As can be seen in Table I, ROMRES has more advantageous features than others.

https://doi.org/10.1017/S0263574721000357 Published online by Cambridge University Press

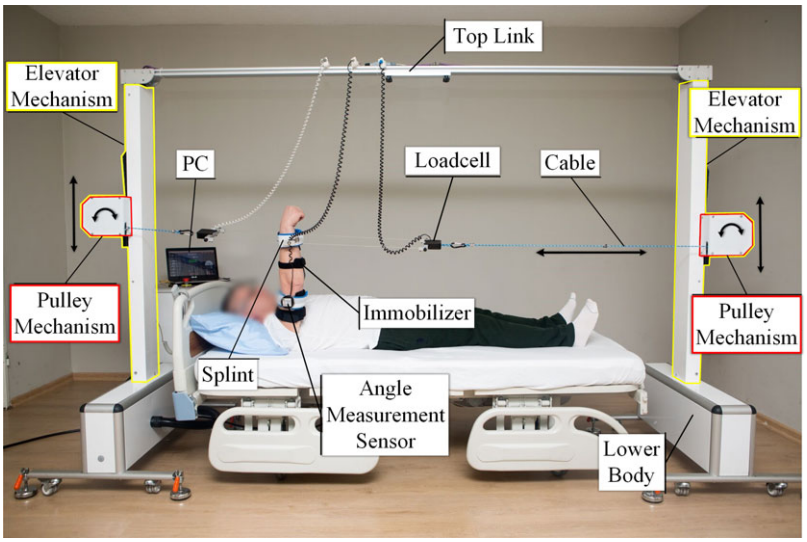

Figure 1. *Components of ROMRES.*

The remainder of the paper is organized as follows: In Section 2, the design of the ROMRES is presented. The system kinematics and dynamics of the robot are introduced in Section 3. In the following section, the design of the controllers is presented. Section 5 covers the experiments done with a dummy arm and a healthy subject and discussions over the results.

2. Mechatronic system description

2.1. Mechanical design

ROMRES consists of two vertically symmetrical parts. Any part includes three groups: the pulley group, the lower body and the elevator system, see Fig. 1. The pulley system consists of a main pulley, a cable wrapped around the pulley and a servo motor that drives the pulley. There are also auxiliary idle pulleys, which guide the cable to be properly wrapped onto the main pulley. The lower body consists of a case including electronics hardware.

During an exercise, the servo motor applies torque to the pulley according to the torque information received from the motion control unit (MCU) to provide a patient to perform a proper exercise. The cable is attached to the splint, which is attached to the patient's extremity, and transmits the generated torque from the servo motor to the patient's joint. In order to prevent unwanted movement from the passive joints during an exercise, an immobilizer is used. For example, during shoulder flexion or extension exercise, the movement of elbow is unwanted. The immobilizer fixes this joint to a predetermined angle. Thus, the angle of the extremity of interest can be more accurately measured.

During the exercise, the angle between the patient extremity and the cables must be adjusted to about 90 degrees in order to increase the range of motion of the limb. The best way to achieve this is to use an elevator system that moves pulley group according to the angle information of the extremity during an exercise.

The cables in this system are made of polypropylene and 3 mm in diameter. With the help of experiments, it has been seen that the change in length of the cable under normal operating loads is $<1\%$. Therefore, it was safe to assume that flexibility of cables does not affect the exercises.

The geometric parameters of the system are shown in Fig. 2. Here, θ is the angular position of the limb; ψ_1 and ψ_2 are angular position of the pulleys at left and right sides, respectively; H_1 and H_2 are linear positions of the elevator mechanisms at left and right sides, respectively; r is the radius of the

https://doi.org/10.1017/S0263574721000357 Published online by Cambridge University Press

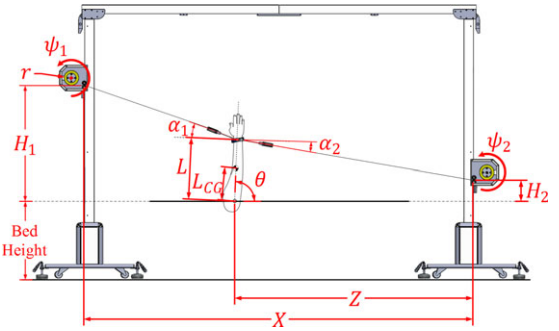

Figure 2. *Geometric parameters of ROMRES.*

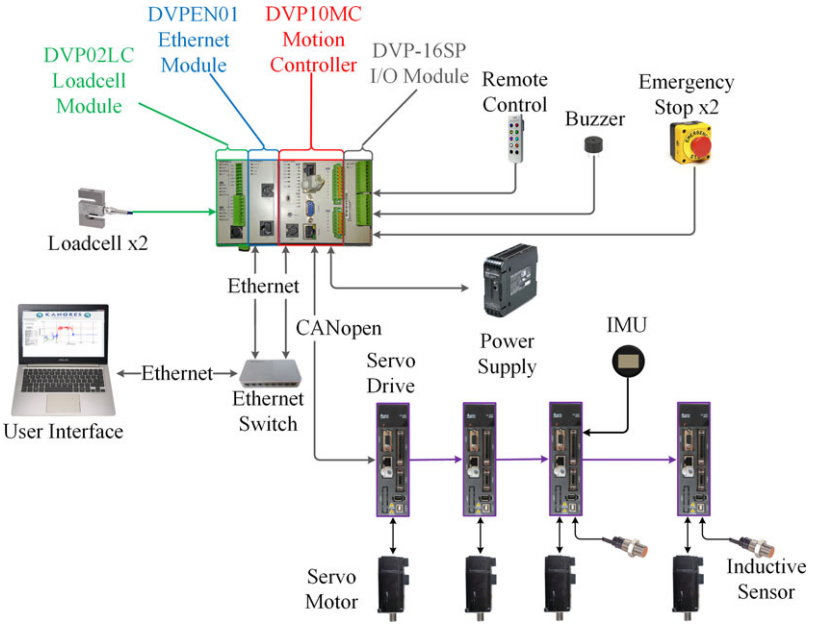

Figure 3. *Electronics diagram of ROMRES.*

pulleys. The horizontal distance between the side pulleys is shown by X, and the horizontal distance between the second pulley and the center of limb joint is denoted with Z. The length of the limb is denoted with L. The distance between the center of gravity of the limb and the limb joint is denoted with L_{CG}. The angle between the normal of the limb and the cable at the left side is denoted with α_1, and the angle between the normal of the limb and the cable at the right side is denoted with α_2.

2.2. Actuators, sensors and control hardware

A diagram consisting of all electronic modules of the ROMRES is shown in Fig. 3. The robot contains a DVP10MC11T (Delta Electronics, Taipei, Taiwan), which is an integrated programmable logic controller (PLC) and the MCU running in real time. Although these are integrated into a single module, they are programmed separately and responsible for different tasks. The MCU controls the servo motors of the robot through the CAN open network and reads the data from the angle measurement unit. The PLC is mainly responsible for storing the data and initializes the start-up parameters, managing the digital input/output (IO) features of the robot and reading the load cell data.

https://doi.org/10.1017/S0263574721000357 Published online by Cambridge University Press

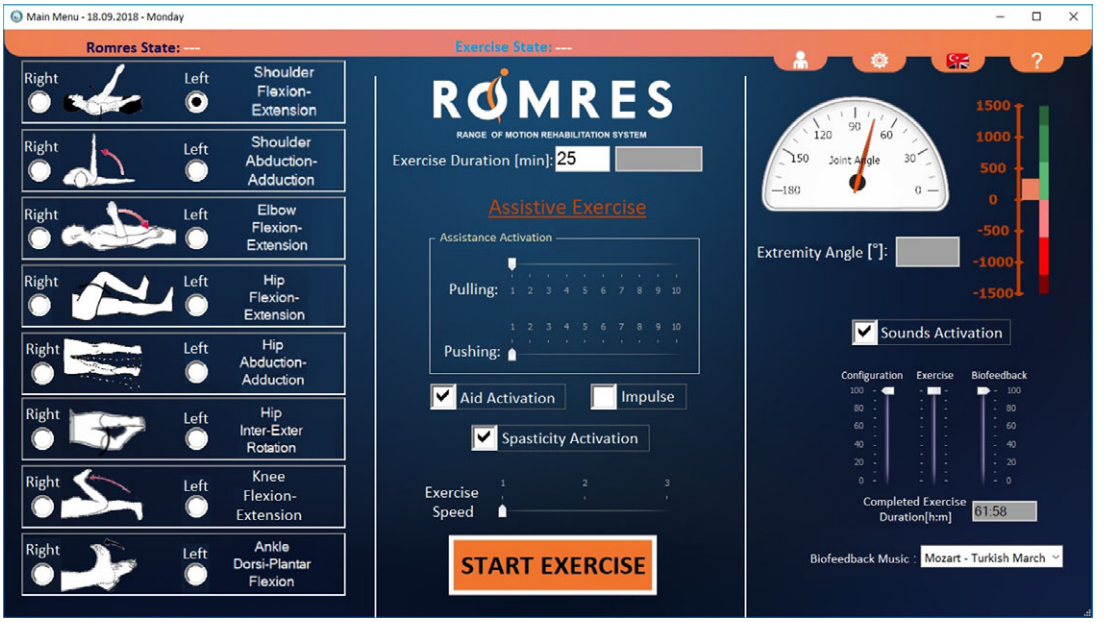

Figure 4. *Graphical user interface.*

A Delta DVP202LC (Delta Electronics, Taipei, Taiwan) load cell module was used to amplify and digitize the signals received from the load cells (Mavin NA32; Hope Technologic Co., Xiamen, China) which were converted to S-type by assembling custom milled parts. Two load cells mounted on both sides of the splint which is directly connected to the extremity to measure the forces acting on the cables. A Delta DVPEN01 (Delta Electronics, Taipei, Taiwan) Ethernet communication module was used to provide a fast and reliable interface between the computer and the PLC/MCU devices.

Four pairs of industrial servo motors/drivers were used to actuate the pulleys and the elevator systems. The Delta ASD-A2-0421M (Delta Electronics, Taipei, Taiwan) servo drivers communicate with the MCU and generate necessary electrical signals to drive the motors with 20-bit incremental encoders (Delta ECMA10604GS; Delta Electronics, Taipei, Taiwan).

A custom-made micro-electro-mechanical system (MEMS) accelerometer (Atek; Alfa Electronics, Istanbul, Turkey)-based inclinometer was used to measure the angle of the patient's extremity around a single axis as an analog signal between 4 and 20 mA. The sensor is attached to the center of the rotation of the limb as close as possible. The aim is to isolate the sensor from linear accelerations. As the sensor is accelerometer-based, the angle readings are affected by any acceleration other than the gravitational one. It is seen that the sensor is able to generate accurate measurements within ± 50 degrees of inclination in the axes other than the one it is designed for. This angle margin is acceptable for the intended usage of the inclinometer in this study.

2.3. Software components

A custom graphical user interface (GUI) application, shown in Fig. 4, was developed in C# programming language to command the robot and monitor its operation. The software contains various patients' information in its accounts. It contains robot configuration parameters related to its operations. The user can select an exercise type, an exercise duration, an exercise speed and an assistance level. The user can start or stop the exercise via the GUI, and he/she can monitor the angle of the patient's extremity during the exercise as well as the applied forces by the patient. The user can change and customize the exercise

https://doi.org/10.1017/S0263574721000357 Published online by Cambridge University Press

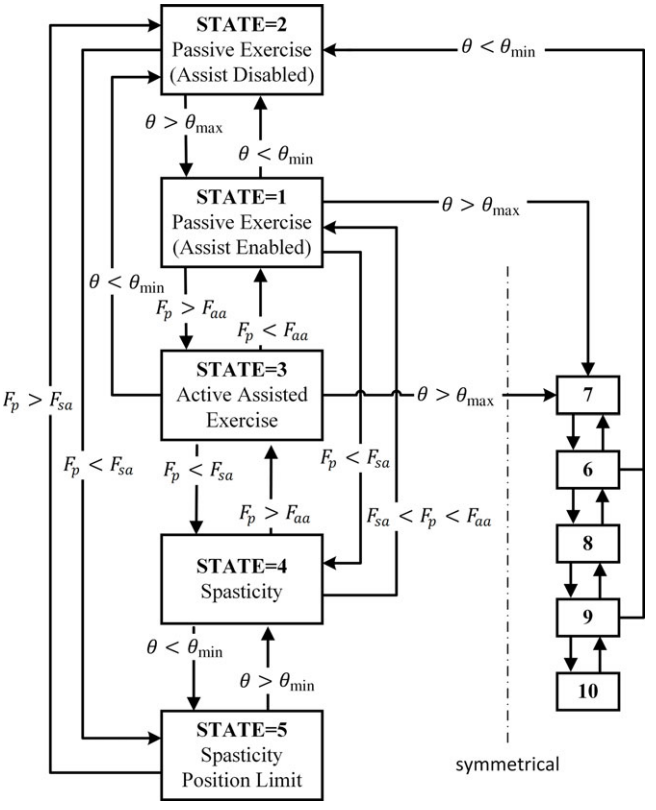

Figure 5. *State machine of ROMRES.*

parameters via options screen when needed. The software can also save the collected data to track the progression of the patient along the rehabilitation process.

The motion controller software contains a state machine, which contains a rule-based structure, and decides the behavior of the pulley motors according to the measured force from the patient. It switches the operation modes of the pulley motors by changing the virtual spring and damper coefficients of the impedance controllers and the velocity reference.

The state machine receives the patient's force as an input and continuously checks whether the patient performs an active movement or a spasticity by comparing the forces generated by the patient with predetermined force thresholds, which are the "assist activation" ($F_{aa} > 0$) and the "spasticity activation" ($F_{sa} < 0$) ones.

The state machine also receives the angle of the extremity and continuously checks whether the extremity angle is within the predetermined minimum angle ($\theta_{\min}$) and maximum angle ($\theta_{\max}$) which are set by healthcare staff. The minimum and maximum angles are the limits of the range of motion in the extension and the flexion directions of the exercise, respectively. When the extremity angle exceeds these limit values, the state is changed to ensure keeping the extremity in the range of motion of the exercise.

The state machine has a total of ten different states, five of which are for the flexion direction and five for the extension one. The block diagram of the state machine is shown in Fig. 5.

1. Passive Exercise Assist-enabled State: This is the state which provides the system to track the given position and velocity reference within the range of motion with a high impedance ($K_{d\,high}$ and $D_{d\,high}$). Additionally, the system makes impulsive movement in reverse direction periodically. The impulsive

https://doi.org/10.1017/S0263574721000357 Published online by Cambridge University Press

movement is similar to the repeated stretch technique of proprioceptive neuromuscular facilitation [45]. In the technique of repeated stretch (repeated contraction), a command is given by the physiotherapist to contract the muscles while they are stretched. Similarly, in ROMRES, during the impulse period, the cables move in the opposite direction to the ongoing motion of the exercise. It switches again to the normal direction at the end of the impulse duration. The impulse duration can be changed by the preferences of the health professionals. However, it is usually set to short time intervals, such as a quarter of a second. It is thought that this impulsive movement has positive effects in the rehabilitation of the patients and is not mentioned further here because it is beyond the scope of this work.

2. Passive Exercise Assist-disabled State: This state is activated when the extremity of the patient is outside of the range of motion. The system brings the extremity into the range of motion by following the position and velocity references with a high impedance.
3. Active-Assisted Exercise State: When the active force applied by the patient exceeds the system's adjusted active force threshold, the system switches to the active-assisted exercise state. In this state, the virtual spring and damper coefficients of the impedance controller are set to low impedance ($K_{d\,low}$ and $D_{d\,low}$).

   When the system works with a low impedance, the part of the impedance control formula depending on the position error reduces its effect. However, the part depending on the external force is applied in the same way. Thus, the controller makes the motors to produce the torque at the rate of applied external force, instead of tracking the given position. If the patient cannot move his/her extremity, this working method enables the controller to increase the amount of assistance until the patient's extremity moves.
4. Spasticity State: Spasticity is involuntary and velocity-dependent muscle tone that causes resistance to movement [46]. When the force applied by the patient is below the spasticity force threshold of the system, it is switched to the spasticity state. The direction of the velocity reference generated in this state is reversed. Thus, it is ensured that the patient's extremity was made to move slowly by resisting to the spasticity. This state continues as long as the patient applies the spasticity force within the range of motion.
5. Spasticity Position Limit State: This state occurs when the patient applies the spasticity force outside the range of motion. The system works in the same way as the Passive Exercise Assist-disabled State does. This state is developed only to observe easily whether the patient applies the spasticity force beyond the range of the joint motion.

These five states (1–5) are used when the system moves the extremity in the flexion (pulling) direction. In the direction of the extension (pushing), the states similar to those in the direction of flexion (6–10) were used.

3. System kinematics and dynamics

3.1. Assumptions

Various assumptions were made in order to simplify the process of mathematical modeling:

- The cables of the robot were assumed to be rigid, since their measured maximum strain in a specific test was $<1\%$.
- The rotational joint position of the patient's limb was assumed fixed in Cartesian coordinates.
- The motion of the system was assumed planar.
- The kinematic model of the system was obtained only for one group of pulley, elevator and limb.
- The elevator mechanisms were assumed simple linear systems.
- The servo motors were assumed ideal.
- The overall mechanical system was assumed frictionless.

https://doi.org/10.1017/S0263574721000357 Published online by Cambridge University Press

3.2. Geometric constraints

The kinematic constraints of the robot are identified as scleronomic holonomic constraints. The equations of these constraints are given as:

$$g_1 := \sqrt{(H_1 - L\sin\theta)^2 + (X - Z + L\cos\theta)^2} - \psi_1 r = 0 \tag{1}$$

$$g_2 := \sqrt{(L\sin\theta - H_2)^2 + (Z - L\cos\theta)^2} - \psi_2 r = 0. \tag{2}$$

3.3. Kinematics

The Jacobian matrix of the system is needed to design the controller. Therefore, using aforementioned constraints, a partial kinematic model was determined by obtaining the Jacobian of the robot. This partial kinematic model includes only one side of the pulley system and elevator group. It shows the relation between the angular velocity of the limb, the angular velocity of the pulley and the linear velocity of the pulley, so that the equation

$$\dot{\theta} = \begin{bmatrix} J_{11} & J_{12} \end{bmatrix} \begin{bmatrix} \dot{\psi}_1 \\ \dot{H}_1 \end{bmatrix} \tag{3}$$

is satisfied. If we isolate θ in (1) and then take its partial derivative with respect to ψ_1, we obtain J_{11}. Similarly, J_{12} was calculated by taking partial derivative of isolated θ with respect to H_1. The Jacobian of the system relative to $\dot{\psi}_2$ and $\dot{H}_2$ can be derived in a similar fashion.

3.4. Dynamics

The Euler–Lagrange method was used because it makes easier to include the constraints by using the Lagrange multipliers. According to Euler–Lagrange method, the dynamics of a system can be written as

$$\frac{d}{dt}\left(\frac{\partial \mathcal{L}}{\partial \dot{q}_i}\right) - \frac{\partial \mathcal{L}}{\partial q_i} = \tau_i + \sum_{j=1}^{k} \lambda_i \frac{\partial g_j}{\partial q_i} \tag{4}$$

where the term $\mathcal{L}$ denotes the Lagrange operator, q_i denotes the generalized coordinates of the system, τ_i denotes the total torques at the generalized coordinates, λ_i denotes the lagrange multipliers and g_j denotes the constraint equations. The generalized coordinates of the system were chosen as ψ_1, H_1, ψ_2, H_2 and θ. Considering previously given assumptions, the total kinetic energy and total potential energy of the system can be written as,

$$T = \frac{1}{2}M_e\dot{H}_1{}^2 + \frac{1}{2}M_e\dot{H}_2{}^2 + \frac{1}{2}I_p\dot{\psi}_1{}^2 + \frac{1}{2}I_p\dot{\psi}_2{}^2 + \frac{1}{2}\left(I_k + M_k L_{CG}^2\right)\dot{\theta}^2 \tag{5}$$

$$V = M_e g H_1 + M_e g H_2 + M_k g L_{CG}\sin\theta \tag{6}$$

where the term M_e denotes the mass of the elevator mechanisms, I_p denotes the inertia of the pulley mechanisms, I_k denotes the inertia of the limb at its center of gravity, M_k denotes the mass of the limb, L_{CG} denotes the distance between the mass center and the joint of the limb and g denotes the gravity. Employing (4), the dynamical equations of the system are obtained as follows:

https://doi.org/10.1017/S0263574721000357 Published online by Cambridge University Press

$$
\begin{aligned}
I_p\ddot{\psi}_1(t) + \lambda_1 r &= \tau_1 \\
M_e\left(\ddot{H}_1\,(t) + g\right) - \frac{\lambda_1 a}{\sqrt{a^2 + (X-b)^2}} &= F_1 \\
I_p\ddot{\psi}_2(t) + \lambda_2 r &= \tau_2 \\
M_e\left(\ddot{H}_2(t) + g\right) - \frac{\lambda_2 c}{\sqrt{c^2 + b^2}} &= F_2 \\
\ddot{\theta}(t)\left(M_k L_{CG}^2 + I_k\right) + M_k g\cos(\theta(t))\, L_{CG} + d + e &= \tau_p
\end{aligned} \tag{7}
$$

where

$$
\begin{aligned}
a &= H_1(t) - L\sin(\theta(t)) \\
b &= Z - L\cos(\theta(t)) \\
c &= H_2(t) - L\sin(\theta(t)) \\
d &= \frac{\lambda_1 L\cos(\theta(t))\,(a) + L\sin(\theta(t))\,(X-b)}{\sqrt{a^2 + (X-b)^2}} \\
e &= \frac{\lambda_2 L\cos(\theta(t))\,(c) - L\sin\,(\theta(t))\,(b)}{\sqrt{c^2 + b^2}}.
\end{aligned}
$$

The terms λ_1 and λ_2 can be eliminated using constraint Eqs. (1) and (2). Two of the resultant equations do not contain any derivative term because the constraint equations are holonomic. It is necessary to take the derivatives of these equations in order to express the dynamics of the nonlinear system in the $\dot{x} = f(x, u)$ form. The state vector of the system is formed as

$$
x = \begin{bmatrix} \psi_1 & \dot{\psi}_1 & H_1 & \dot{H}_1 & \psi_2 & \dot{\psi}_2 & H_2 & \dot{H}_2 & \theta & \dot{\theta} \end{bmatrix}^T.
$$

4. Controller design

Overall controller block diagram of ROMRES is given in Fig. 6.

4.1. Pulley controller

The performances of the position control algorithms depend on the accuracy and the sensitivity of the sensors. A MEMS-based angle measurement unit was used to measure the angle of the extremity in the system. Not only delayed but also noisy data were received from this sensor. Therefore, the encoder positions of the motors instead of the angle of the extremity are used in the control algorithm because the resolution of the encoders is 20-bit and the encoder feedback has a less delay and a less noise than the feedback of angle measurement unit does. According to the requirements of the exercises, the pulley motors should follow the reference, which is determined by the trajectory generator. It is well known that the motors should not operate in a rigid position control mode, but they should follow a position in compliance with the patient's reactions. In the given circumstances, the impedance controller was found suitable as a control method for the controller of the pulley motors. The purpose of the impedance control method is to obtain a controller force that can establish a mathematical relation between the external force and the position tracking error [47]. Although this relation may vary according to the studies carried out, it is generally expressed by using the second-order equation given as:

$$
M_d\ddot{e} + D_d\dot{e} + K_d e = \tau_e \tag{8}
$$

https://doi.org/10.1017/S0263574721000357 Published online by Cambridge University Press

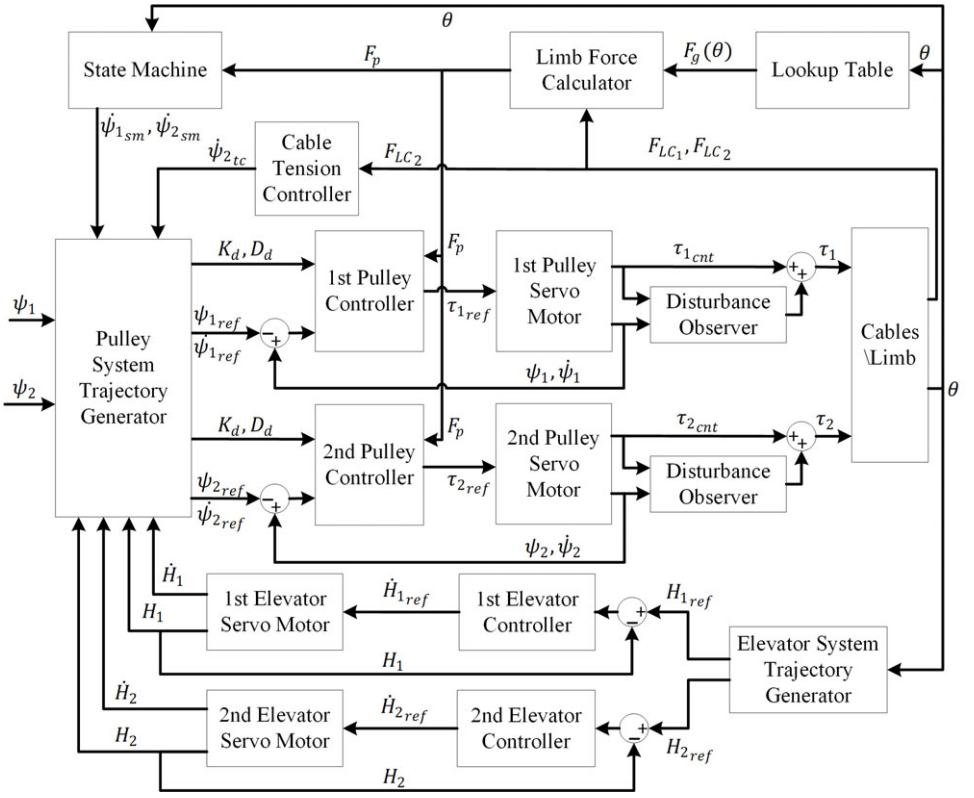

Figure 6. *Overall controller block diagram of ROMRES.*

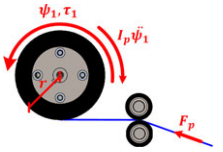

Figure 7. *Free body diagram of the pulley system.*

where the terms M_d, D_d and K_d are the desired inertia, damping and spring coefficients of the system, respectively. The τ_e term denotes the external torque, and e denotes the difference between the actual and desired positions.

Figure 7 illustrates the free body diagram of the pulley system, where τ_1 is the torque of the pulley motor and F_p is the external force applied by the patient. It has been assumed that no other external forces affect the pulley. Friction forces are not included in the impedance control algorithm since those forces have been compensated by a disturbance observer algorithm.

The dynamical model of the pulley system according to Fig. 7 is given as:

$$I_p\ddot{\psi}_1 = \tau_1 - F_p r. \tag{9}$$

The main equation of the controller has been adapted to the system in the form of (10) in order to establish a mathematical relationship between the force applied by the patient and the position tracking error as

$$M_d\ddot{e} + D_d\dot{e} + K_d e = -F_p r \tag{10}$$

https://doi.org/10.1017/S0263574721000357 Published online by Cambridge University Press

The position tracking error indicates the difference between the position reference and the position of the pulley motor. This value can be shown as:

$$e = \psi_1 - \psi_{1_{ref}}. \tag{11}$$

The acceleration tracking error is obtained by taking a double derivative of (11) as:

$$\ddot{e} = \ddot{\psi}_1 - \ddot{\psi}_{1_{ref}}. \tag{12}$$

Substituting (12) into (10) yields:

$$M_d\left(\ddot{\psi}_1 - \ddot{\psi}_{1_{ref}}\right) + D_d\dot{e} + K_d e = -F_p r. \tag{13}$$

The desired acceleration is considered to be zero ($\ddot{\psi}_{1_{ref}} = 0$). Thus, (13) is rearranged as:

$$\ddot{\psi}_1 = \frac{\left(-F_p r - (D_d\dot{e} + K_d e)\right)}{M_d}. \tag{14}$$

If (14) is substituted into (9), then,

$$\frac{I_p}{M_d}\left[-F_p r - (D_d\dot{e} + K_d e)\right] = \tau_1 - F_p r \tag{15}$$

is obtained. If some arrangements are made on (15), the general controller equation becomes

$$\left(1 - \frac{I_p}{M_d}\right) F_p r - \left(\frac{I_p}{M_d}\right)(D_d\dot{e} + K_d e) = \tau_1 \tag{16}$$

In most studies in the relevant literature, the reference trajectories of the rehabilitation robots are usually designed to move the patients' limbs under the influence of a certain speed and force within certain position limits [48, 49]. In this study, some simple trajectories, similar to the ones given in refs. [50, 51, 52, 53, 54], were designed for demonstrating the robot to successfully perform three exercises mentioned above. Basically, they serve to perform the movements shown in Fig. 1 within the chosen ranges of motion, speed and force. They are also expected to satisfy the required criteria, such as switching to the active assistance state when needed.

The state machine generates constant velocity references for the pulleys depending on the current state, but tracking these references with pulleys is not enough for the limb to move with a constant speed. While a pulley controls the length of a cable, the pulley is moved vertically by an elevator that makes the cable perpendicular to the limb. This coupled motion of the pulley causes the limb to have an undesired effect which must be compensated during an exercise. The compensation is possible with the Jacobian matrix given in the kinematic analysis of the system. By using the Jacobian matrix, the effect of elevator mechanism is calculated and the velocity reference of the pulley is updated accordingly.

The equations for the velocity and the position references of the first pulley controller are given as:

$$\dot{\psi}_{1_{ref}} = \dot{\psi}_{1_{sm}} + \dot{\psi}_{1_{comp}} \tag{17}$$

$$\psi_{1_{ref}} = \psi_{1_{IC}} + \int \dot{\psi}_{1_{ref}} dt \tag{18}$$

where the subscript '1' denotes the first pulley; the terms $\dot{\psi}_{1_{ref}}$ and $\psi_{1_{ref}}$ represent the angular velocity and position references for the pulley controller, respectively; $\dot{\psi}_{1_{sm}}$ is the velocity reference generated by the state machine; $\psi_{1_{Ic}}$ represents the initial angular position of the pulley and $\dot{\psi}_{1_{comp}}$ is the calculated compensation velocity reference to minimize the effect of elevator motions on the limb. Similar equations can be applied to the second pulley system. Only difference is the additional velocity reference

https://doi.org/10.1017/S0263574721000357 Published online by Cambridge University Press

($\psi_{2_{tc}}$) fed from cable tension controller. The equations for the velocity and the position references of the second pulley controller are given as

$$\dot{\psi}_{2_{ref}} = \dot{\psi}_{2_{sm}} + \dot{\psi}_{2_{comp}} + \dot{\psi}_{2_{tc}} \tag{19}$$

$$\psi_{2_{ref}} = \psi_{2_{IC}} + \int \dot{\psi}_{2_{ref}} dt \tag{20}$$

The formula

$$\dot{\psi}_{1_{comp}} = -\frac{\dot{H}_1 J_{12}}{J_{11}} \tag{21}$$

describes the compensation velocity reference.

The velocity reference $\dot{\psi}_{1_{sm}}$ is fed to the trajectory generator from the state machine, see Fig. 6. The state machine handles the direction of movement by checking the angle information that is fed back from the angle measurement sensor. If a maximum or minimum angle is reached, the state is switched and an appropriate velocity reference is generated by the new state. This velocity reference is constant most of the time during each state. There is an exception for assist-enabled state which they handle the optional impulsive motion by reversing the exercise direction for short periods of time. To reverse the exercise direction, they simply reverse the velocity reference they normally generate. The constant velocity references for each state can be configured by the user via GUI.

4.2. Cable tension controller

In order to provide the patient's comfort during an exercise, the cables should not be too tense. On the other hand, if they are too loose, the patient's extremity cannot be moved in the direction of the exercise. In addition to this, to be able to excite the limb promptly in the reverse direction to the ongoing motion, slackness of the cable on the trailing side needs to be avoided. For this reason, a PD controller has been used to keep the tension of the cables within a certain range during an exercise. The designed controller is combined with the pulley system controllers in a cascade control structure. The second load cell output (F_{LC_2}) is fed to the tension controller as input. The controller outputs a velocity reference ($\dot{\psi}_{2_{tc}}$), which is used in the pulley system trajectory generator in order to keep the tension value close to a preset constant reference, see Fig. 6. Thus, during flexion for example, if the tension on the cable of the second load cell exceeds the reference, the second pulley is accelerated in the direction of movement of the exercise; hence, tension is reduced. Likewise, if the tension on the cable of the second load cell falls below the reference, the pulley velocity is slowed down and the tension is increased to the desired level.

The output of this controller was saturated between ± 0.8 times of the exercise speed. Thus, the second pulley is prevented from changing direction due to the tension controller during the exercise.

The tension reference is set via GUI. This value is optimized by trial and error to maximize the patient's comfort under the consultancy of healthcare staff. An example value of 4000 gf is used throughout the experiments in this study.

4.3. Limb force calculator

In order to calculate the force applied by the patient, two load cells were attached to the cables at both sides of the limb. The free body diagram of the limb isolated from the rest of the system is shown in Fig. 8.

Applying Newton's Second Law of Motion for rotation, the following equation can be obtained:

$$I_l \ddot{\theta} = \left(F_{LC1} \cos \alpha_1 - F_{LC_2} \cos \alpha_2\right) L + F_p L - F_g(\theta) L \tag{22}$$

https://doi.org/10.1017/S0263574721000357 Published online by Cambridge University Press

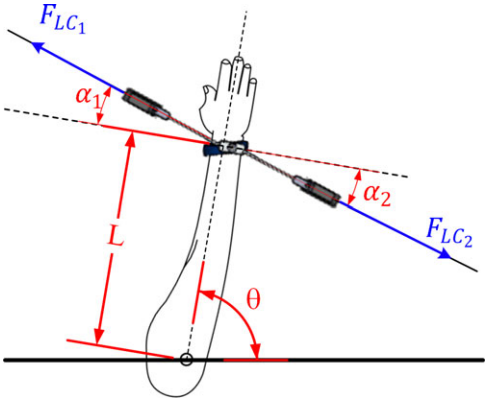

Figure 8. *Free body diagram of the limb.*

where the term $F_g(\theta)$ is the effect of weight of the limb on the cables. In (22), it is assumed that $\ddot{\theta} = 0$. If the force applied by the patient F_p is isolated in the resulting equation, it is obtained as:

$$F_p = \left(F_{LC_2}\cos\alpha_2 \; - F_{LC1}\cos\alpha_1\right) - F_g(\theta). \tag{23}$$

Due to the diversity of patients, the mass and center of gravity of the limb may vary on a vast scale. Also, measuring these parameters is not practical. Therefore, a procedure was developed to measure $F_g(\theta)$ term. In this procedure, the patient is asked to relax and apply no force for one full cycle of the exercise. During this cycle, it is assumed $F_p = 0$ and $F_g(\theta)$ is calculated from (23) relative to θ. Then, $F_g(\theta)$ is stored in a lookup table. After one cycle of the exercise, at each iteration of calculation, $F_g(\theta)$ is obtained from the lookup table and F_p is calculated from (23).

The robot continuously checks the tension level on the cables via the load cells. A predetermined tension level is maintained by adjusting the velocity reference of the second pulley. By doing so, the necessary planar motion can be provided most of the time, since the tension on the cables does not allow the limb to tilt in the orthogonal direction. If a joint shifts from its original position however, the robot continues the exercise, while the limb is slightly tilted. Under these circumstances, the performance of the limb force calculator degrades, and so the patient needs to apply more force in order the robot to switch to the assistive mode.

4.4. Elevator controller

The primary purpose of the elevator system is to make the cables as perpendicular as possible to the limb axis at all times. To accomplish this, elevator mechanisms continuously position themselves during an exercise according to the limb angle.

An elevator mechanism contains a timing belt/pulley mechanism and an industrial servo driver/motor system. This servo system can be driven by feeding velocity references to the driver. The servo driver then can generate necessary electrical signals and send them to the motor according to predetermined ramping parameters. In this study, the ramping parameters were chosen very small, so that they are ignored; therefore, the dynamics of the servo system are supposed to be ideal. The elevator mechanisms were modeled at a basic level. The validation and the verification of its controller and trajectory generator were done through simulations before implementing them in the actual system.

APD controller was chosen as the control law for the elevator mechanisms as follows:

$$\dot{H}_{1_{ref}} = C_p e_{H_1} + C_d \dot{e}_{H_1} \tag{24}$$

where the terms C_p and C_d are the proportional and derivative controller gains, respectively. e_{H1} is the error between the reference and actual heights of the first elevator mechanism. The actual height of the

https://doi.org/10.1017/S0263574721000357 Published online by Cambridge University Press

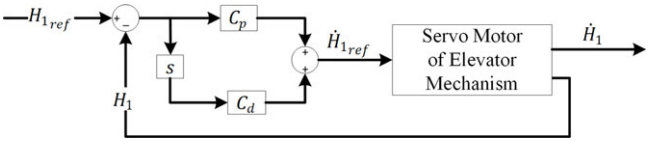

Figure 9. *Block diagram of elevator mechanism controller.*

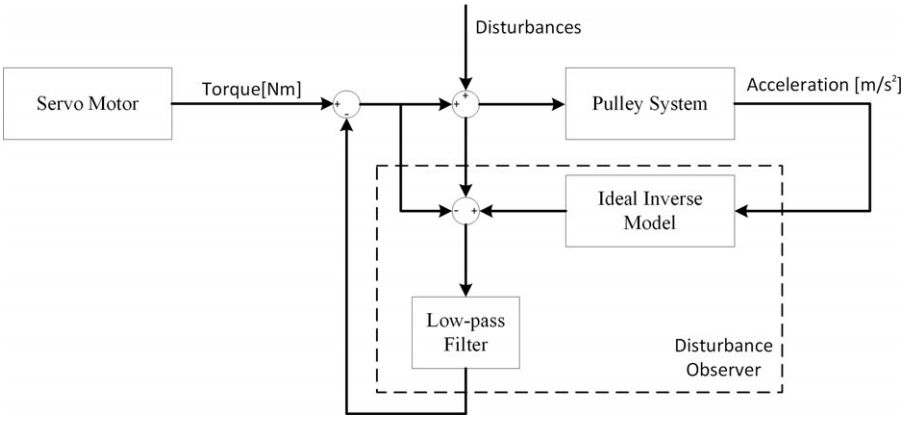

Figure 10. *Block diagram of disturbance observer model.*

elevator can be calculated from the encoder of the servo motor. The block diagram of the controller is given in Fig. 9. The control law for the second elevator mechanism was derived in a similar fashion.

In order the elevator system to properly work, the reference signals of the controllers must be generated at each control cycle. These reference signals indicate that the required ideal heights of the pulley mechanisms for the cables to be perpendicular to the extremity. In order to achieve it, a trajectory generator, which calculates the position of the elevator mechanisms cyclically using various geometric calculations based on the position of the patient limb, was developed.

In Fig. 2, α_1 and α_2 denote the angles between the cable and the normal vector of the patient's extremity. As previously discussed, the aim here is to maintain these angles close to zero. Thus, the geometric calculations of the desired elevator heights are calculated as:

$$H_{1_{ref}} = L\sin\theta + (X - Z + L\cos\theta)\tan(\pi - \theta) \tag{25}$$

$$H_{2_{ref}} = L\sin\theta + (Z - L\cos\theta)\tan(\pi - \theta). \tag{26}$$

These generated height references are given as inputs to the PD controllers of the elevator servo motors.

4.5. Disturbance observers

Preliminary studies indicated that a variable friction exists due to the mechanical structure of the system. Some experimental studies were carried out to obtain a friction model. However, the desired sensitivity cannot be achieved with that friction model, especially for an active-assisted exercise. To overcome this problem, a disturbance observer was designed. The ideal inverse model of a pulley system has been established. Ideally, the pulley systems are modeled as frictionless and consisting of motors, reducers and idle pulleys which can only rotate with the motor torque. The block diagram of the disturbance observer model is given in Fig. 10.

The ideal model of the system can be given as:

$$T_{ideal} = I\ddot{\psi} \tag{27}$$

https://doi.org/10.1017/S0263574721000357 Published online by Cambridge University Press

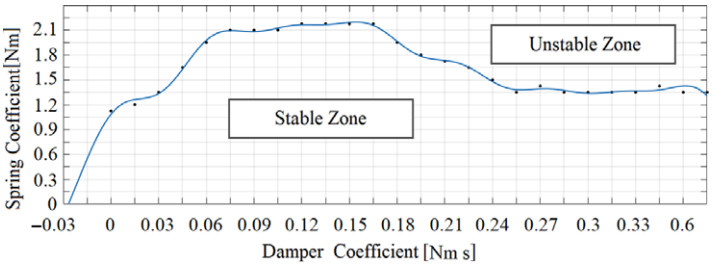

Figure 11. *Stable and unstable zones of the controller.*

where T_{ideal} is the torque which is required to accelerate the pulley system in ideal conditions. This equation is expressed by including the friction as:

$$T_{motor} = T_{ideal} + T_{friction}. \tag{28}$$

Thus, the torque value for friction and the other disturbances is determined by

$$T_{friction} = T_{motor} - T_{ideal}. \tag{29}$$

A low-pass filter was used to reduce the effect of high-frequency noises.

5. Experimental studies

5.1. Determining stable region of the controller

Finding the virtual spring and damper coefficient ranges, in which the impedance control algorithm can operate stably, is of importance. Once the appropriate ranges of the coefficients have been found, the spring and damper coefficients can be selected according to the desired working stiffness. Experimental methods can be used to find the range of coefficients for the modern algorithms such as an impedance controller [55, 56]. According to the results of the experiments, the spring and damper coefficient ranges can be found and the coefficients of the controller can be freely and accordingly chosen [56, 57].

In the experiments, it has been found that 0.08 Nm intervals in the spring coefficient were significant. Thus, the spring coefficient was increased at an interval of 0.08 Nm. Likewise, 0.016 Nm s intervals in the damper coefficient were found to be significant.

According to the test procedure, the system was operated with no load, as the controller virtual spring and damper coefficients were initially set to zero. A step input was sent as the position reference to the controller, and then, the spring coefficient was increased by 0.08 Nm until the motors could reach the given reference position. This process was repeated until the system continuously oscillates. When the system becomes unstable, the spring coefficient was recorded and reset. Next, the damper coefficient was increased by 0.016 Nm s, and the same process was repeated.

The zones where the system performs as stable and unstable are shown in Fig. 11. Here, the range of damper coefficients in which the spring coefficient range is the largest between 0.06 and 0.16 Nm s in the stable zone. When the damper coefficient is over 0.24 Nm s, the position tracking performance decreases due to a high damping and the motors cannot reach the given input value. For this reason, the area, which the damper coefficient is above 0.24 Nm s, is out of the working range.

5.2. Experiments with motorized dummy arm

In order to objectively test the system's performance and safely, a dummy arm was designed. A single-DOF human arm-shaped test dummy with a servo motor and a PLC was developed and realized. The experimental setup is shown in Fig. 12.

https://doi.org/10.1017/S0263574721000357 Published online by Cambridge University Press

Table II. *Numerical values of all parameters.*

Parameter	Value	Unit	Parameter	Value	Unit
L	0.46	m	X	2.53	m
θ_{min}	60	deg	θ_{max}	120	deg
$K_{d\,high}$	6.6×10^{-7}	Nm	F_{aa}	0.05	Nm
$D_{d\,high}$	0.25×10^{-7}	Nm s	F_{sa}	-1	Nm
M_d	1×10^{-5}	Kg m^2	I	1.5×10^{-5}	kg m^2
$K_{d\,low}$	2.6×10^{-8}	Nm	w	7.2	°/s
$D_{d\,low}$	0.5×10^{-8}	Nm s	H_{bed}	0.68	m
H_{1max}	0.7	m	H_{1min}	0.15	m
H_{2max}	0.7	m	H_{2min}	0.15	m

Figure 12. *Experimental setup for assessing performance of the system.*

Several different tests have been conducted during the development process. The artificial patient's force, F_p', was generated through the servo motor of the dummy arm. To evaluate the performance of the robot, F_p' has been compared with F_p, which is calculated by the robot, using the force information received from the load cells. Also, the encoder data of the dummy arm have been compared with the angle measurement sensor data to evaluate the performance of the angle sensor.

The exercise type was "left shoulder flexion-extension". The assist activation and spasticity activation parameters were adjusted by trial and error under the consultancy of physiotherapists. The maximum and minimum angle limits of the exercises were adjusted in a way maximizing the range of motion while not compromising the performance of the device too much. If, for example, the limits were to be chosen too high or too low, the elevator mechanisms would not be able to keep the cables at 90 degrees to the limb because of the mechanical limitations. This would have negatively affected the performance of the device and the comfort of the patient. Also, the speed of the exercise (w) was adjusted under the consultancy of physiotherapists when exercising with a real human subject. The numerical values of all the parameters are given in Table II. The preliminary results with this test setup were reported in ref. [58]. The results of four experimental scenarios for the system are separately examined below. The experimental data obtained from these three exercises have been tabulated and exhibited in Appendix B.

5.2.1. Passive exercise experiment

The first experiment conducted on the system is the passive exercise. In this experiment, the motorized dummy arm does not apply any external force to the system. In this case, the first performance criterion

https://doi.org/10.1017/S0263574721000357 Published online by Cambridge University Press

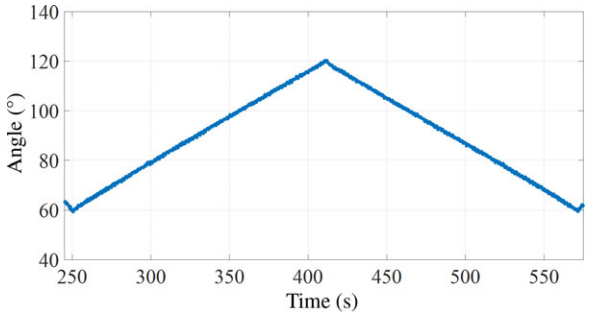

Figure 13. *Passive exercise experiment: Extremity position.*

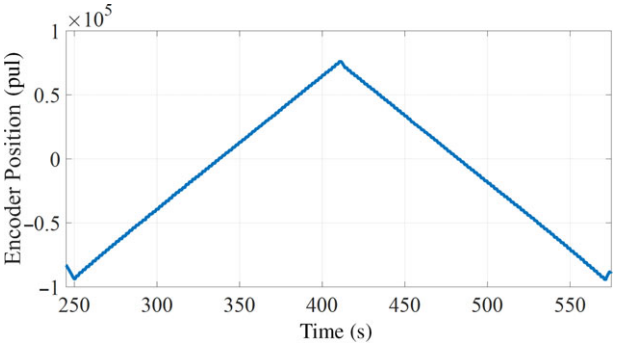

Figure 14. *Passive exercise experiment: Encoder position of dummy arm.*

is to check whether the system switches into active assistance state on its own by making a faulty active force detection at any point. The second performance criterion is to check whether the movement of elevator systems affects the dummy arm during the exercise. The third criterion is to ensure that the system gets the exercises done within the given angle limits. The last criterion is to check whether the system can get the impulsive movement accurately done. The data received from the angle measurement sensor for passive motion are shown in Fig. 13.

The plot in Fig. 13 shows the data obtained from the angle measurement unit directly attached to the dummy arm. The plot indicates one round of an exercise, and the system is able to exercise the patient joint at the specified angle range. Second, it is seen that the extremity position increases or decreases at a constant rate. It is understood that elevators are properly moved. However, the impulsive movement cannot be distinguished in this plot. The main reasons of this are the small delay and noisy results received from the angle measurement sensor. Furthermore, an experienced physiotherapist suggests that decreasing the magnitude and increasing the frequency of the impulsive movement yield better results.

Although the impulsive movement is not clearly demonstrated in the data received from the angle measurement sensor, it can be observed in the encoder data obtained from the dummy arm as seen in Fig. 14.

The system completed one cycle of passive exercise in approximately 5 min. For a clearer view, the impulsive movement is zoomed in as shown in Fig. 14. Here, the encoder position of the test apparatus changes in the positive direction over time. However, this movement stops periodically, and a smaller movement in the negative direction occurs. A similar movement can be seen in the time history of both pulley motor positions as shown in Fig. 15.

In these graphs, the reason why the motor position and position references do not appear straight as in the patient's extremity position is due to the algorithm compensating the effect of vertical movement of elevator systems on the extremity. This algorithm instantly changes the pulley motor position reference

https://doi.org/10.1017/S0263574721000357 Published online by Cambridge University Press

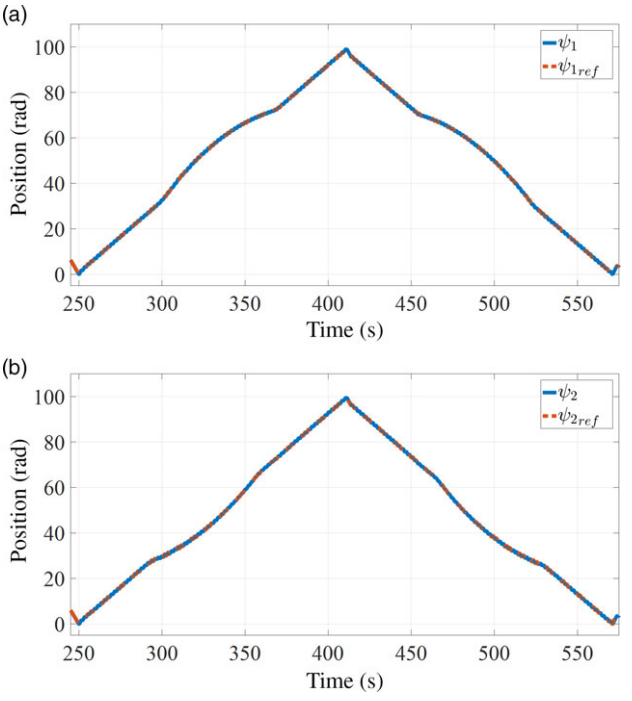

Figure 15. *Passive exercise experiment: (a) first and (b) second motor positions and position references.*

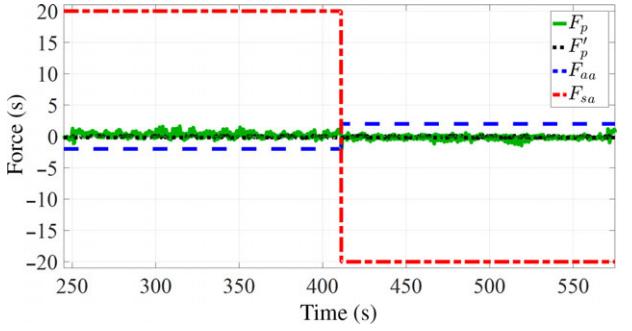

Figure 16. *Passive exercise experiment: Applied and measured external forces.*

according to the elevator motor speed using (21), so the elevator motor effects on the patient's extremity can be compensated. The motors move in the pulling direction until the 410th s. Up to this point, the first pulley motor provides the movement by pulling the cable, while the second pulley motor releases the cable with a certain amount of resistance, so that the tension on the cable is maintained.

Figure 16 shows the external force measured by the ROMRES and the external force applied to the system through the motor of the dummy arm. No command was given to the motorized dummy arm, so it did not apply any force to the system. Therefore, the graph only shows the noise values. The system obtains the external force applied by comparing the data of two load cells located in the splint mechanism. Since the data obtained from these load cells are noisy, the external force applied to the system is calculated with oscillations within ± 1 N. However, these oscillations do not cause any problem since their amplitudes are below 2 N, which is the smallest threshold value to switch into the active-assisted exercise state.

https://doi.org/10.1017/S0263574721000357 Published online by Cambridge University Press

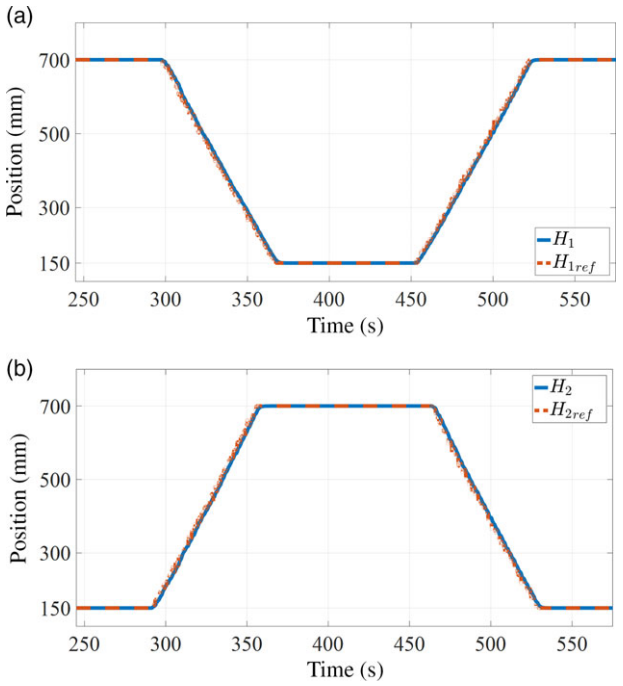

Figure 17. *Passive exercise experiment: (a) the first and (b) the second elevator positions and position references.*

Figure 17 shows the positions of the elevator system motors. The graphs show noise and fluctuations around reference values between 150 and 700 mm. The fluctuations are due to the impulsive movements, but the noise is caused by the algorithm that generates the reference based on the angle measurement sensor. By designing a PD controller that follows the reference with a small delay, the motor was ensured not to follow the noises occurring in the reference value and the patient's comfort was maintained.

5.2.2. Assisted exercise experiment

The second experiment conducted on the system is the active-assisted exercise. In this experiment, the test apparatus applies a force on the system at certain points. The purpose of this experiment is to test whether the system successfully detects the active force and switches to the active-assisted exercise state, when the test apparatus exerts a force to the system in the direction of the movement. The data received from the angle measurement unit for active-assisted exercise are shown in Fig. 17(a).

Just like passive exercise experiment, the system operated between 60 and 120 degrees in the active-assisted exercise experiment. However, unlike the passive exercise extremity position graph, jumps can be seen at certain points, where the test apparatus applies an active force to the system. For a better clarity, the measured external force and force values obtained from the motor of the dummy arm are shown at the bottom plot in Fig. 18.

As seen in Fig. 18, when external force applied to the system that exceeds 2 N in the direction of the movement, the system stops following the passive exercise trajectory and let the dummy arm continue the movement. These graphs also reveal that although there is a noise in the external force caused by the sensors, the system can detect an externally applied active force.

The pulley motors' positions for an active-assisted exercise are shown in Fig. 19. Since one of the position plot of the motors is sufficient to convey the characteristics of the motion, the second one is omitted hereafter.

https://doi.org/10.1017/S0263574721000357 Published online by Cambridge University Press

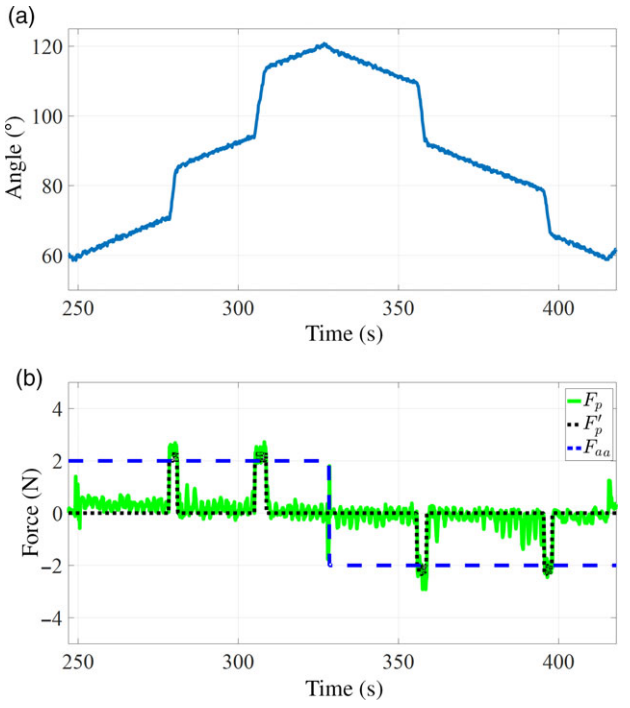

Figure 18. *Assisted exercise experiment: Relationship between (a) extremity angle and (b) external force.*

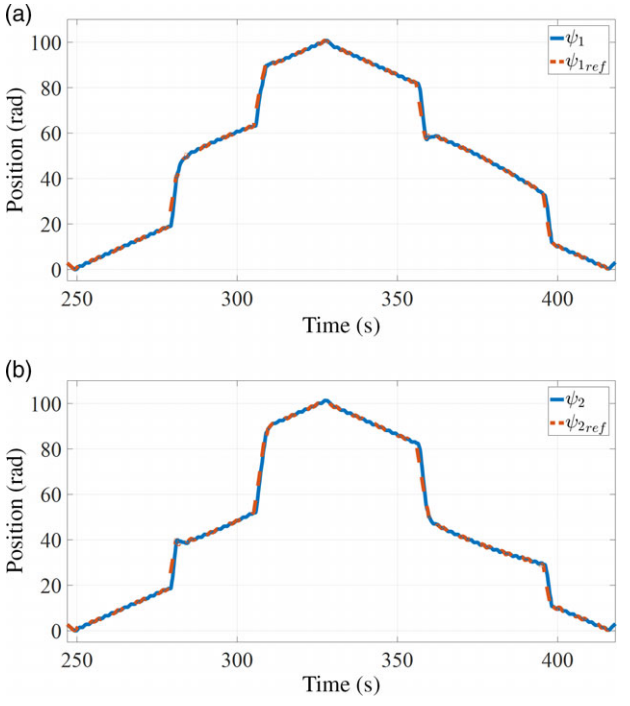

Figure 19. *Assisted exercise experiment: (a) the first and (b) the second motor positions and position references.*

https://doi.org/10.1017/S0263574721000357 Published online by Cambridge University Press

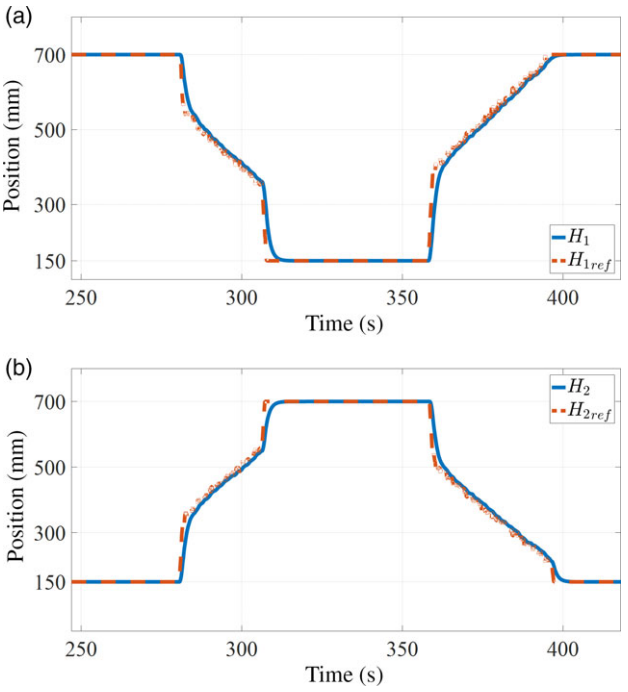

Figure 20. *Assisted exercise experiment: (a) first and (b) second elevator positions and position references.*

The graphs show that the pulley motors follow the position reference as long as the dummy arm does not apply any external force to the system. When the motorized dummy arm applies an active force to the system, the motors follow the rapidly increasing position reference with some delay. The main reason for this delay is that the control system makes the virtual spring and damper coefficients very low to allow only a small amount of support. Not a big difference occurred between the motor position reference and the actual motor position, since the dummy arm is lightweight and constantly applies a force. However, a bigger difference can be seen in the experiments with healthy human subjects as shown in Fig. 32.

Figure 20 shows the elevator positions. Although these graphs are basically the same as the graphs obtained during passive exercise, there is a difference in the reference values due to the rapid angle changes during an active movement. However, the controller's performance was not affected by those rapid changes.

5.2.3. Spasticity exercise experiment

In this scenario, an external force of approximately 20 N is applied to the system in the opposite direction of movement at certain points. The aim of this experiment is to imitate an extremity with spasticity in the dummy arm and to observe the response of the system in the state of a spasticity. Data obtained from the angle measurement sensor and the measured external force are shown in Fig. 21.

In Fig. 21, it can be seen that while the system is moved in the pulling (positive) direction, the direction of the movement is changed between 1050 and 1080th s as the system is switched to the spasticity state. Similarly, the system was exposed to a spasticity between 1250 and 1260th s during the pushing (negative) movement.

As seen in the graphs, when the external force exceeded 20 N in the opposite direction of movement, the system is stopped following the passive exercise trajectory and then started to move in the opposite direction without an impulse. In this situation, the behavior of the pulley motor is clearly shown in Fig. 22.

https://doi.org/10.1017/S0263574721000357 Published online by Cambridge University Press

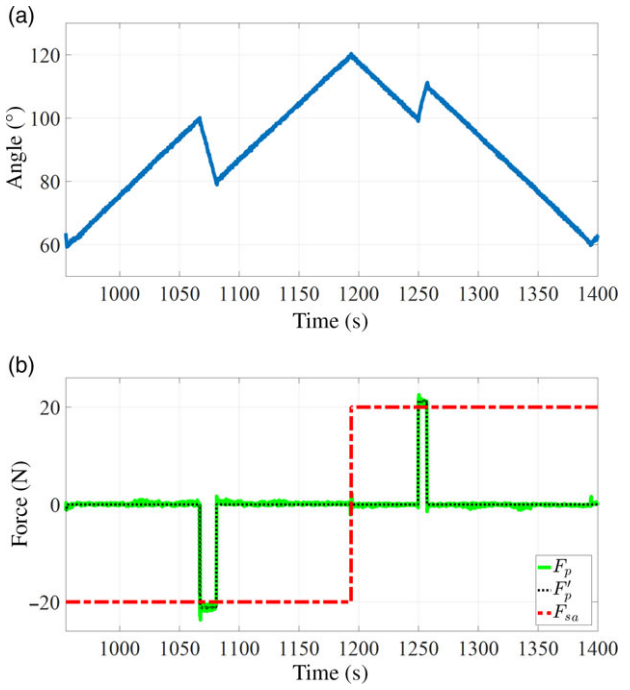

Figure 21. *Spasticity exercise experiment: Relationship between (a) extremity position and (b) external force.*

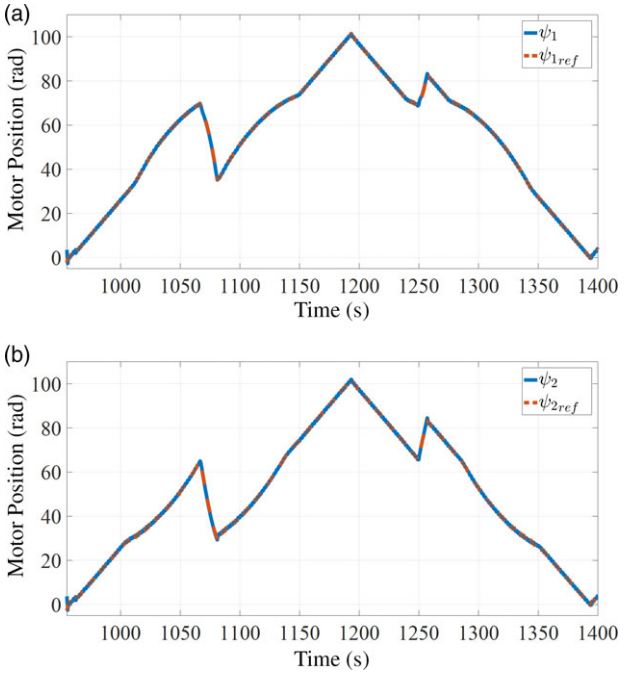

Figure 22. *Spasticity exercise experiment: (a) first and (b) second motor positions and position references.*

https://doi.org/10.1017/S0263574721000357 Published online by Cambridge University Press

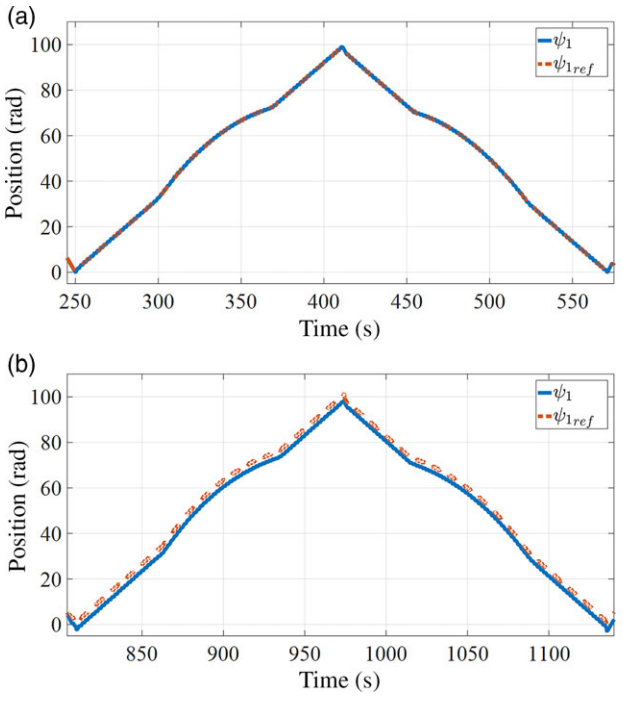

Figure 23. *Passive exercise (a) with and (b) without disturbance observer.*

It can be seen that the pulley motor followed the position reference as in the passive movement before the application of the external force. When the external force is applied on the system by the dummy arm in the opposite direction of the movement, the pulley motors continue to follow the position reference in the opposite direction. In the spasticity state, the position reference is generated without the impulsive movement.

5.2.4. Evaluation of disturbance observer performance

A disturbance observer was designed to eliminate the effects of the friction and some disturbances on the system operation. In this study, the operating performances of the system in the cases of passive exercise, active-assisted exercise and exercise on spasticity were observed with and without using the disturbance observer. Since the disturbance observer affects only the pulley motors, the pulley motor position graphs will be sufficient to assess the system performance when the disturbance observer does not work.

The motor position and the position reference of the first pulley motor for the passive exercise with and without the disturbance observer are shown in Fig. 23. When the plots are examined, it can be seen that the difference between the position and position reference values of the motor is significant, when the disturbance observer does not work. Therefore, the disturbance observer has a positive effect on the position tracking performance.

A more significant effect of the disturbance observer can be seen in Fig. 24. When the disturbance observer is off, the position of the dummy arm under the action of the active force does not change. The reason is why that the 2 N active force applied by the dummy arm is not enough to move itself by overcoming the friction. The use of the disturbance observer has a substantial effect on the active-assisted exercise.

Similar to the performance of the disturbance observer in the passive exercise, a positive effect was also observed in the exercise on the spasticity.

https://doi.org/10.1017/S0263574721000357 Published online by Cambridge University Press

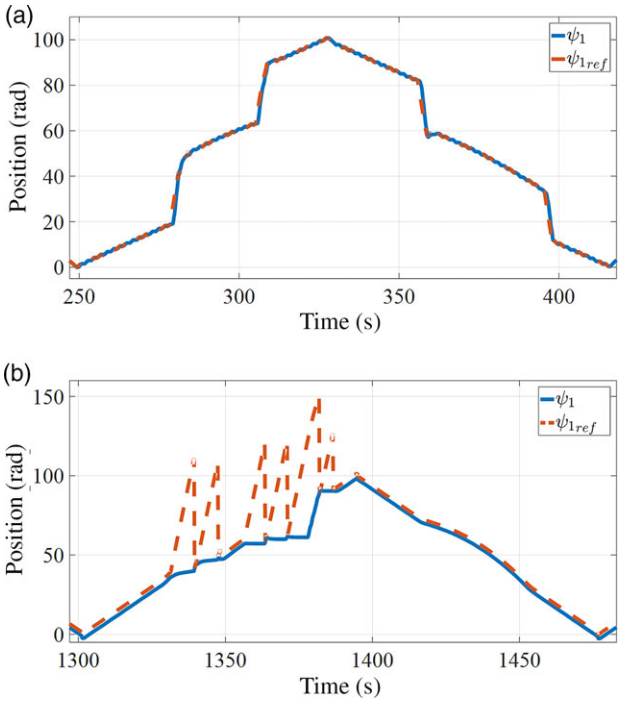

Figure 24. *Active-assisted exercise (a) with and (b) without disturbance observer.*

5.3. Experiments with healthy subject

In order to test the performance of the robot, some experiments with a healthy subject were conducted. The subject was male, 175 cm tall and weighed 70 kg. The exercise type was selected as "left elbow flexion-extension" from the user interface software. The assist activation (F_{aa}) and the spasticity activation (F_{sa}) parameters were adjusted by trial and error under the consultancy of the physiotherapists. The numerical values of the parameters were almost the same as they were in experiments with dummy arm. Only $\theta_{\max} = 120°$, $\theta_{\min} = 60°$, $H_{1\max} = 0.53$ m, $H_{1\min} = 0.15$ m, $H_{2\max} = 0.3$ m and $H_{2\min} = 0$ m were specifically chosen. The experimental setup is shown in Fig. 25. The results of three experimental scenarios performed on the system are discussed in the following sections.

5.3.1. Passive exercise experiment

In this experiment, no external force is applied by the subject. The procedure followed here is the same as in the passive exercise experiment performed with the motorized dummy arm. The biggest advantage of the experiments done with the motorized dummy arm is that the force applied by the dummy arm on the system was known and it could be compared with the external force measured by the system. Because the force applied by the subject cannot be measured during the experiments, only the external force data measured by the system are included in our analysis. The data received from the angle measurement unit for one cycle of passive exercise are shown in Fig. 26.

As seen in Fig. 26, the system was able to exercise the human subject's extremity within the specified angle range. Second, it is seen that the extremity position increases or decreases at a constant rate. This shows that elevators operated as expected. It is also seen that the impulse speed is slightly increased in this operation mode. Thus, the impulsive movement has become distinguishable in the data received from the angle measurement sensor.

https://doi.org/10.1017/S0263574721000357 Published online by Cambridge University Press

Figure 25. *The experimental setup for the experiments with the healthy subject.*

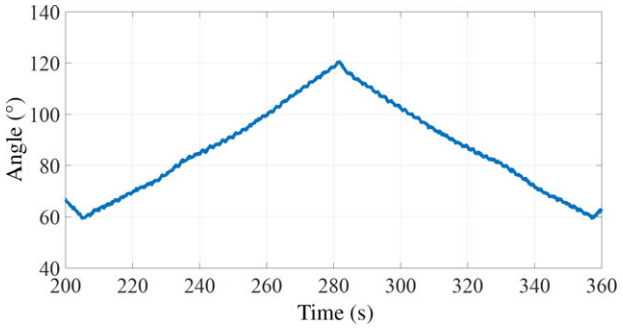

Figure 26. *Passive exercise experiment on healthy subject: Extremity position.*

As seen in Fig. 27, the motors move in the pulling direction until the 281st s. Up to this point, the first pulley motor pulls the extremity, while the second one releases the cable with a certain amount of resistance, so that the tension on the cable is maintained.

Figure 28 shows the torque values of the first and the second motors. The graphs show the torque value of the 1st motor varies between 0.3 and 0.4 Nm. The torque value of the 2nd motor varies between -0.3 and -0.2 Nm. There is an increase in motor torque values compared to the passive exercise with the motorized test dummy. The reason for this is that the extremity of the person is heavier than the dummy arm.

Figure 29 shows the external force values measured by the system. The subject was instructed not to apply any force. For this reason, force value measured by the system is only the noise values. The system calculates the applied external force by comparing the data of two load cells located in the splint mechanism. Since the data received from these load cells are noisy, the external force applied to the system oscillates within ± 1 N.

Figure 30 shows the position and position reference values of the elevator system motors. No difference was observed compared to the experimental study conducted with the dummy arm. Fluctuations

https://doi.org/10.1017/S0263574721000357 Published online by Cambridge University Press

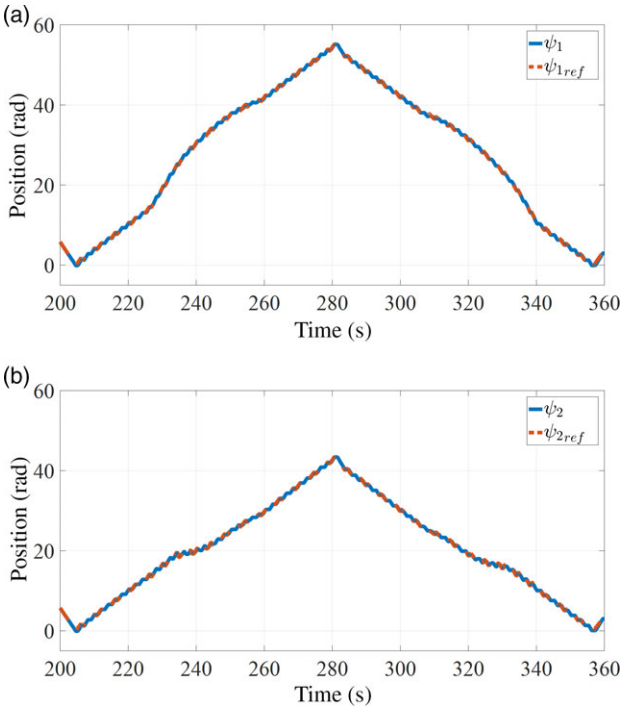

Figure 27. *Passive exercise experiment on healthy subject: (a) The first and (b) the second motor positions and position references.*

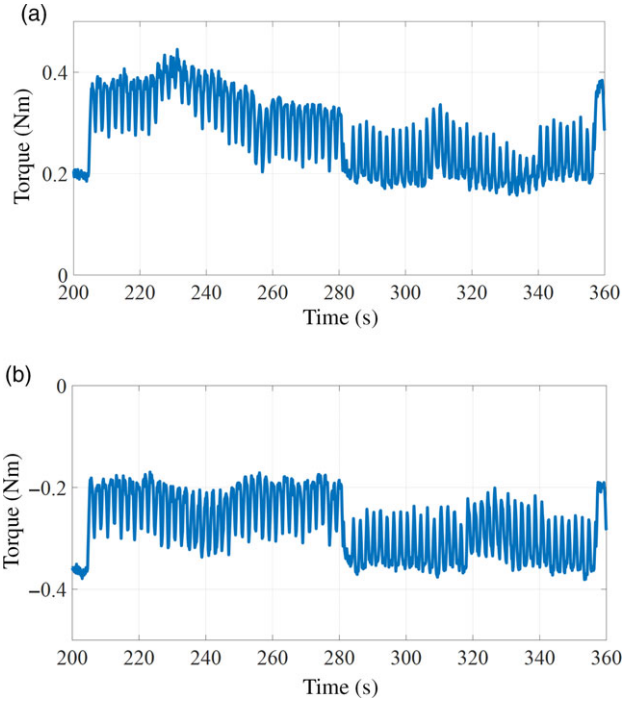

Figure 28. *Passive exercise experiment on healthy subject: (a) the first and (b) the second motor torque values.*

https://doi.org/10.1017/S0263574721000357 Published online by Cambridge University Press

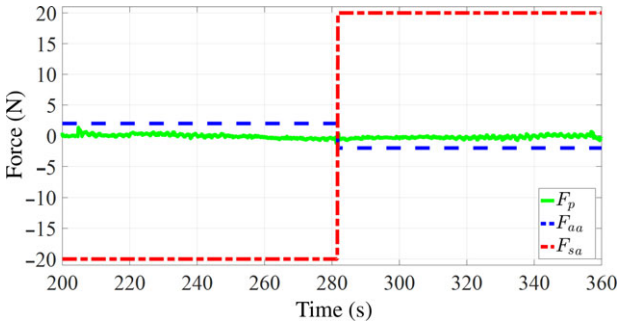

Figure 29. *Passive exercise experiment on a healthy subject: External force measured by the device.*

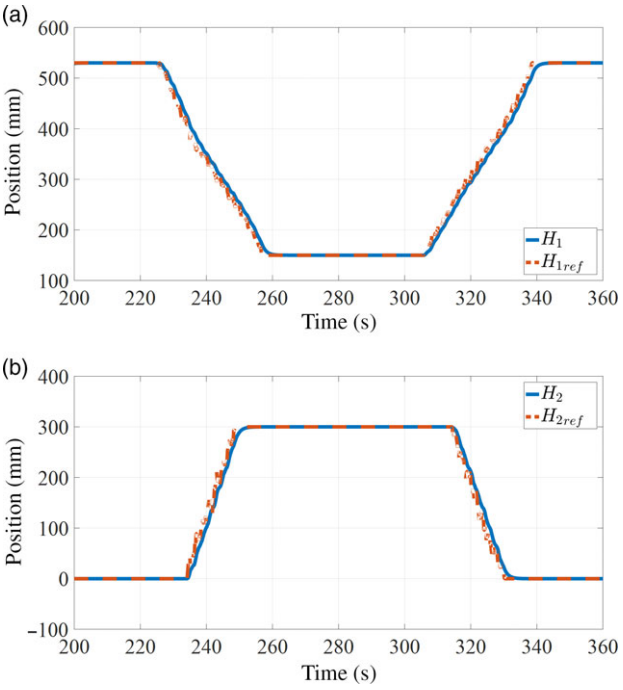

Figure 30. *Passive exercise experiment on healthy subject: (a) the first and (b) the second elevator positions and position references.*

and noises in motor references occurred similarly. By designing a PD controller that follows the reference with a small delay, the motor was ensured not to follow the noises occurring in the reference value and the human subject's comfort was maintained.

5.3.2. Assisted exercise experiment

In this experiment, the subject exercised by the system applies a force in the direction of the movement at certain points. The purpose of this experiment is to test whether the system successfully detects the force and switches into the active-assisted exercise state. The data received from the angle measurement sensor for active-assisted movement are shown in Fig. 31.

Unlike the passive exercise extremity position graph, there are jumps at 368 and 375th s due to the force applied by the subject. There is no difference between this result and the one obtained in the experiment conducted with the dummy arm.

https://doi.org/10.1017/S0263574721000357 Published online by Cambridge University Press

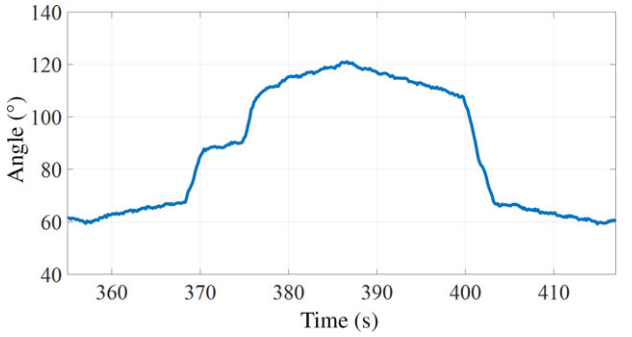

Figure 31. *Assisted exercise experiment on healthy subject: Extremity position.*

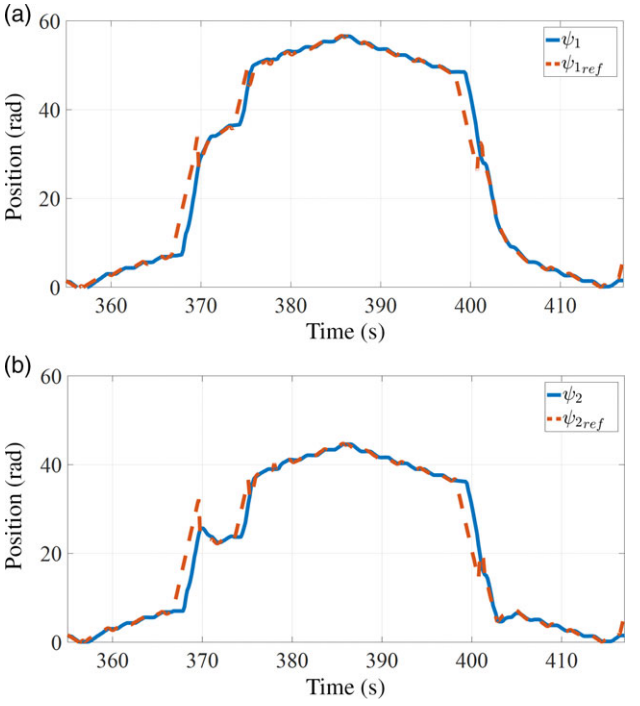

Figure 32. *Assisted exercise experiment on healthy subject: (a) the first and (b) the second motor positions, position references.*

In Fig. 32, a significant difference can be observed compared to the plot in Fig. 18. The pulley motors precisely tracked the position reference, when no active force was applied on the system. However, when the system is switched into the active-assisted exercise state, a delay occurred between the position reference and the motor positions. The main reason for this delay is that the system makes the virtual spring and damper coefficients smaller in the active-assisted exercise state to let the human subject perform the movement as much as possible. A certain time after the active movement begins, the system increases the level of the assistance until the extremity of the person starts moving. The extremity moves with a constant assistance level, while the position and the speed references increase.

Figure 33 shows the motor torques during an active-assisted exercise. When the subject does not apply a force, the graph fluctuates in the same way as in the passive movement. However, when the subject

https://doi.org/10.1017/S0263574721000357 Published online by Cambridge University Press

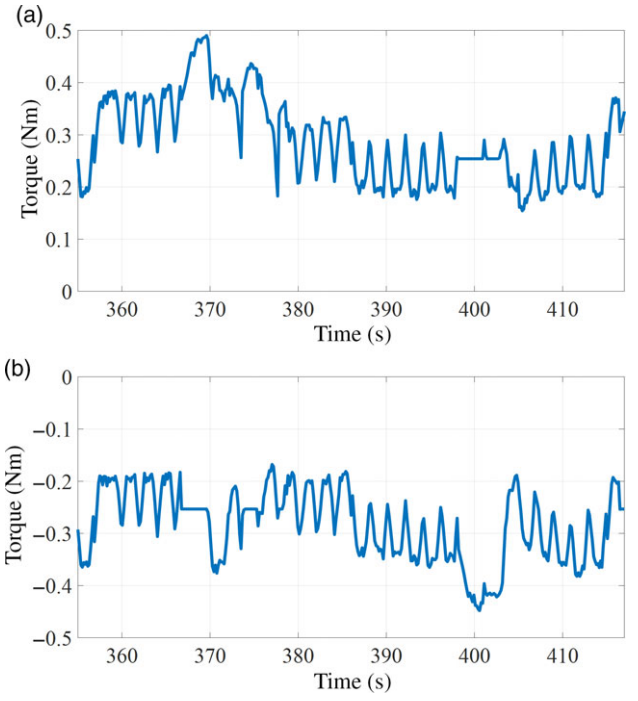

Figure 33. *Assisted exercise experiment on healthy subject: (a) first and (b) second motor torques.*

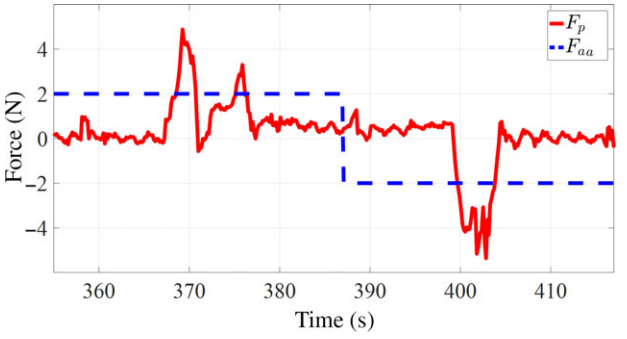

Figure 34. *Assisted exercise experiment on human: External force.*

applies an active force, the motor torque stops fluctuating and the torque value increases proportional to the applied force as seen in Fig. 34.

5.3.3. Exercise on spasticity experiment

According to this scenario, the subject exercised by the system applies approximately 20 N force in the opposite direction of the movement at certain points. The purpose of this experiment is to observe the response of the system in the state of a spasticity.

As shown in Fig. 35, while the system moves in the pulling (positive) direction between the 460 and 475th s, the robot changes its direction by switching to the state of spasticity. Similarly, the system was exposed to the spasticity between 575 and 585th s during the pushing (negative) movement.

Figure 36 shows the external force measured by the system and the threshold value of the spasticity. As shown in this graph, the external force exceeded the threshold values at certain times.

https://doi.org/10.1017/S0263574721000357 Published online by Cambridge University Press

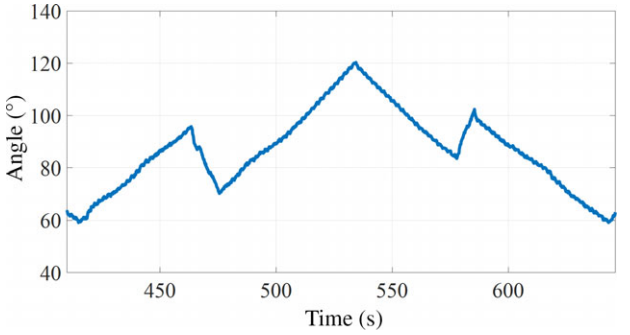

Figure 35. *Spasticity experiment on human: Extremity position.*

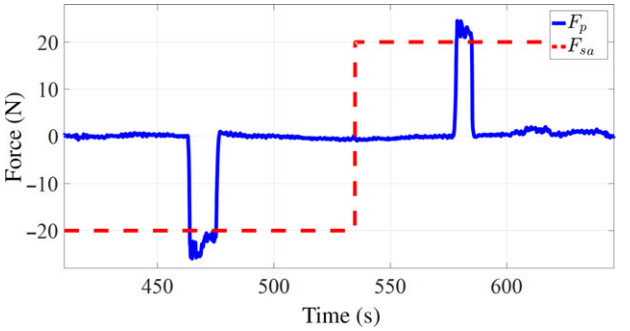

Figure 36. *Spasticity experiment on human: External force applied on the device.*

5.4. Discussion and conclusion

In this study, the mechanical and electronic design, the working mechanism and the control algorithm of the rehabilitation robot ROMRES have been presented. The ROMRES consists of a novel mechanical structure among the rehabilitation robots available in literature. Three main exercise types have been identified for the operation of the robot: the passive exercise, the active-assisted exercise and the exercise for a spasticity. In the passive exercise case, the robot exercises the patient's extremity at a constant speed. In the active-assisted exercise, the patient is required to move his or her extremity, but cannot do it by his/her own. Then, the robot assists the patient to perform the exercise. The last type is the exercise for a spasticity. The spasticity is strong muscle contractions in opposite direction as a reaction to increase in velocity of the joint. When strong muscle contractions in the opposite direction to the exercise occurs, the robot detects this behavior and complies with the patient, allowing him or her to move the limb in the direction of the spasticity.

The first study to ensure that the robot can operate in accordance with these three requirements is the mathematical modeling. At this stage, some simplifications and assumptions have been made and the partial kinematic and dynamic models of the robot have been obtained. Based on the system model, the control system has been designed. PD controllers have been used to control the elevator mechanisms, and an impedance controller has been implemented to control the cables connected to an extremity of the human subject. A state machine structure has been used to make the robot operate in accordance with the exercise requirements. A disturbance observer has been designed mainly to compensate the friction. In particular, the disturbance observer has improved the performances of the system by increasing the sensitivity of the active-assisted exercise. In addition, an algorithm has been developed to calculate the force applied by the human subject. This algorithm can distinguish the human subject's force from

https://doi.org/10.1017/S0263574721000357 Published online by Cambridge University Press

the actuator and gravitational forces. Also, a PD controller has been implemented to maintain a fixed tension level on the cables during the exercise.

The performance of the robot has been assessed using a motorized dummy arm at first. Scenarios have been created to test whether requirements are met. The performance of the robot has also been tested with a healthy subject. When the results of both case studies were examined, it has been seen that the proposed control system successfully controlled the robot and met the requirements.

The load cells have not been able to measure the force resulting from the acceleration terms in the force equation. Therefore, some errors have occurred in the algorithm of the extremity force detection. The performance of the control system can be improved by using torque sensors connected to the pulley systems instead of the load cells. On the other hand, the external disturbance effects on the weight measurement can be reduced by using intelligent or adaptive algorithms. As a result of the trade-off between the comfort and performance of the human subject, his or her joint is not restricted during the exercises. Therefore, if the joint is moved, the performance of the calculator algorithm for the limb force degrades.

The cable-driven robot ROMRES provides significant advantages: (1) it can be configured easily for exercising different articulations such as shoulders, hips, knees and ankles; (2) it does not require any orthosis; (3) it does not restrict the natural DOFs of the human limbs; (4) the effect of the weight of the limb on the cables is determined and taken into account by the software; (5) the applied force to the limb through the cables can be kept constant as the limb rotates with respect to its joint and (6) the fact that the patient's contact with the robot is only through a splint ensures that the rehabilitation is both comfortable and simple. Thanks to these features, preparation time can be kept short and a natural rehabilitation can be provided by this novel rehabilitation robot.

Acknowledgment. This work was supported by The Scientific and Technological Research Council of Turkey, Ankara, under the grant number TEYDEB-7161164.

Conflicts of Interest The authors declare none.

References

[1] A. L. Behrman and S. J. Harkema, "Physical rehabilitation as an agent for recovery after spinal cord ınjury," *Phys. Med. Rehabil. Clin. North Am.* **18**(2), 183–202 (2007).
[2] R. S. Calabrò, A. Cacciola, F. Bertè, A. Manuli, A. Leo, A. Bramanti, A. Naro, D. Milardi and P. Bramanti, "Robotic gait rehabilitation and substitution devices in neurological disorders: where are we now?," *Neurol. Sci.* **37**(4), 503–514 (2016).
[3] D. Cafolla, R. Matteo and G. Carbone, "Design of CUBE, a Cable-Driven Device for Upper and Lower Limb Exercising," **In:** *New Trends in Medical and Service Robotics* (Springer, Cham, 2019) pp. 255–263.
[4] D. Cafolla, R. Matteo and G. Carbone, "CUBE, a cable-driven device for limb rehabilitation," *J. Bionic Eng.* **16**(3), 492–502 (2019).
[5] L. Peng, Z. G. Hou, L. Peng, L. Luo and W. Wang, "Robot assisted rehabilitation of the arm after stroke: Prototype design and clinical evaluation," *Sci. China Inf. Sci.* **60**(7), 073201 (2017).
[6] R. Colombo, "Performance Measures in Robot Assisted Assessment of Sensorimotor Functions," **In:** *Rehabilitation Robotics* (Academic Press, 2018) pp. 101–115.
[7] C. H. Guzmán, A. Blanco, J. A. Brizuela and F. A. Gómez, "Robust control of a hip–joint rehabilitation robot," *Biomed. Signal Process. Control* **35**, 100–109 (2017)
[8] G. B. Prange, M. J. A. Jannink, C. G. M. Groothuis-Oudshoorn, H. J. Hermens and M. J. Ijzerman, "Systematic review of the effect of robot-aided therapy on recovery of the hemiparetic arm after stroke," *J. Rehabil. Res. Dev.* **43**(2), 171–184 (2006).
[9] G. Fazekas, M. Horvath, T. Troznai and A. Toth, "Robot-mediated upper limb physiotherapy for patients with spastic hemiparesis: A preliminary study," *J. Rehabil. Med.* **39**(7), 580–582 (2007).
[10] H. I. Krebs, M. Ferraro, S. P. Buerger, M. J. Newbery, A. Makiyama, M. Sandmann, D. Lynch, B. T. Volpe and N. Hogan, "Rehabilitation robotics: Pilot trial of a spatial extension for MIT-Manus," *J. Neuroeng. Rehabil.* **1**(1), 5–20 (2004).
[11] P. S. Lum, C. G. Burgar, P. C. Shor, M. Majmundar and M. Van der Loos, "Robot-assisted movement training compared with conventional therapy techniques for the rehabilitation of upper-limb motor function after stroke," *Arch. Phys. Med. Rehabil.* **83**(7), 952–959 (2002).

https://doi.org/10.1017/S0263574721000357 Published online by Cambridge University Press

[12] T. Nef, M. Mihelj and R. Riener, "ARMin: A robot for patient-cooperative arm therapy," *Med. Biol. Eng. Comput.* **45**(9), 887–900 (2007).
[13] T. Nef, V. Klamroth-Marganska, U. Keller and R. Riener, "Three-Dimensional Multi-Degree-of-Freedom Arm Therapy Robot (ARMin)," **In:** *Neurorehabilitation Technology*, 2nd edn. (Springer International Publishing, 2016) pp. 351–374.
[14] M. Bolliger, R. Banz, V. Dietz and L. Lünenburger, "Standardized voluntary force measurement in a lower extremity rehabilitation robot," *J. Neuroeng. Rehabil.* **5**(1), 23 (2008).
[15] L. Lünenburger, G. Colombo and R. Riener, "Biofeedback for robotic gait rehabilitation," *J. Neuroeng. Rehabil.* **4**(1), 1–11 (2007).
[16] J. F. Veneman, R. Kruidhof, E. E. G. Hekman, R. Ekkelenkamp, E. H. F. Van Asseldonk and H. Van Der Kooij, "Design and evaluation of the LOPES exoskeleton robot for interactive gait rehabilitation," *IEEE Trans. Neural Syst. Rehabil. Eng.* **15**(3), 379–386 (2007)
[17] M. H. Jali, N. E. S. Mustafa, T. A. Izzuddin, R. Ghazali and H. I. Jaafar, "ANFIS-PID controller for arm rehabilitation device," *Int. J. Eng. Technol.* **7**(5), 1589–1597 (2015).
[18] J. Wu, J. Huang, Y. Wang, K. Xing and Q. Xu, "Fuzzy PID Control of a Wearable Rehabilitation Robotic Hand Driven by Pneumatic Muscles," *2009 IEEE International Symposium on Micro-NanoMechatronics and Human Science* (2009) pp. 408–413.
[19] W. Meng, Q. Liu, Z. Zhou, Q. Ai, B. Sheng and S. S. Xie, "Recent development of mechanisms and control strategies for robot-assisted lower limb rehabilitation," *Mechatronics* **31**, 132–145 (2015).
[20] M. K. Kirihara, P. N. Saga and D. N. Saito, "Design and control of an upper limb rehabilitation support device for disabled people using a pneumatic cylinder," *Ind. Rob. Int. J.* **37**(4), 354–363 (2010).
[21] C. Ott, R. Mukherjee and Y. Nakamura, "Unified İmpedance and Admittance Control," *2010 IEEE International Conference on Robotics and Automation* (2010) pp. 554–561.
[22] B. Ugurlu, M. Nishimura, K. Hyodo, M. Kawanishi and T. Narikiyo, "Proof of concept for robot-aided upper limb rehabilitation using disturbance observers," *IEEE Trans. Hum. Mach. Syst.* **45**(1), 110–118 (2015).
[23] Ö. Kalkan, *Sinir sistemi hasarları ile ilgili hastalıkların tedavisinde kullanılmak üzere mekanizma* (*Turkish Patent Institute*, 2013) 2013/11368.
[24] A. Alamdari and V. Krovi, "Robotic Physical Exercise and System (ROPES): A Cable-Driven Robotic Rehabilitation System for Lower-Extremity Motor Therapy," *Proceedings of the ASME International Design Engineering Technical Conferences and Computers and Information in Engineering* (2015) p. V05AT08A032.
[25] X. Jin, X. Cui and S. K. Agrawal, "Design of a Cable-Driven Active Leg Exoskeleton (C-ALEX) and Gait Training Experiments with Human Subjects," *Proceedings of the International Conference on Robotics and Automation* (2015) pp. 5578–5583.
[26] Y. Wang, K. Wang, W. Wang, Z. Han and Z. Zhang, "Appraisement and analysis of dynamical stability of under-constrained cable-driven lower-limb rehabilitation training robot," *Robotica*, 1–14 (2020).
[27] I. B. Hamida, M. A. Laribi, A. Mlika, L. Romdhane, S. Zeghloul and G. Carbone, "Multi-objective optimal design of a cable driven parallel robot for rehabilitation tasks," *Mech. Mach. Theory* **156**,104141, 1–24 (2021).
[28] R. S. Gonçalves, T. Alves, G. Carbone and M. Ceccarelli, "Cable-Driven Robots in Physical Rehabilitation: From Theory to Practice," **In**: *Advanced Robotics and Intelligent Automation in Manufacturing* (2020) pp. 52–96.
[29] X. Li, Q. Yang and R. Song, "Performance-based hybrid control of a cable-driven upper-limb rehabilitation robot," *IEEE Trans. Biomed. Eng.* **68**(4), 1351–1359 (2021).
[30] N. Pop, I. Ulinici, D. Pisla and G. Carbone, "Motion Generation for a Cable Based Rehabilitation Robot," *European Conference on Mechanism Science* (2020) pp. 432–439.
[31] Y. Wang, K. Wang and Z. Zhang, "Design, comprehensive evaluation, and experimental study of a cable-driven parallel robot for lower limb rehabilitation," *J. Braz. Soc. Mech. Sci. Eng.* **42**(7), 1–20 (2020).
[32] Y. Wang, K. Wang, Z. Zhang and Z. Mo, "Control strategy and experimental research of a cable-driven lower limb rehabilitation robot," *Proc. Inst. Mech. Eng. Part C J. Mech. Eng. Sci.* (2020). https://doi.org/10.1177/0954406220952510.
[33] S. W. Hwang, J. Bak, J. Yoon and J. H. Park, "Oscillation reduction and frequency analysis of under-constrained cable-driven parallel robot with three cables," *Robotica* **38**(3), 375–395 (2020).
[34] H. Xiong and X. Diao, "A review of cable-driven rehabilitation devices," *Disability Rehabil. Assistive Technol.* **15**(8), 885–897 (2020).
[35] J. D. Sanjuan, A. D. Castillo, M. A. Padilla, M. C. Quintero, E. E. Gutierrez, I. P. Sampayo, J. R. Hernandez and M. H. Rahman, "Cable driven exoskeleton for upper-limb rehabilitation: A design review," *Rob. Auto. Syst.* **126**, 103445 (2020).
[36] X. Jin, D. I. Jun, X. Jin, J. Seon, A. Pott, S. Park, J. O. Park and S. Y. Ko, "Upper Limb Rehabilitation Using a Planar Cable-Driven Parallel Robot with Various Rehabilitation Strategies," **In:** *Cable-Driven Parallel Robots* (Springer, Cham, 2015) pp. 307–321.
[37] D. Zanotto, G. Rosati, S. Minto and A. Rossi. "Sophia-3: A semiadaptive cable-driven rehabilitation device with a tilting working plane," *IEEE Trans. Rob.* **30**(4), 974–979 (2014).
[38] J. Niu, Q. Yang, X. Wang and R. Song, "Sliding mode tracking control of a wire-driven upper-limb rehabilitation robot with nonlinear disturbance observer," *Front. Neurol.* **8**, 646 (2017).

[39] G. Rosati, P. Gallina and S. Masiero, "Design, implementation and clinical tests of a wire-based robot for neurorehabilitation," *IEEE Trans. Neural Syst. Rehabil. Eng.* **15**(4), 560–569 (2007).
[40] G. Rosati, P. Gallina, S. Masiero and A. Rossi, "Design of a New 5 DOF Wire-Based Robot for Rehabilitation," *9th International Conference on Rehabilitation Robotics, 2005. ICORR 2005*, Chicago, IL, USA (2005) pp. 430–433.
[41] R. S. Gonçalves, J. C. M. Carvalho, J. F. Ribeiro and V. V. Salim, "Cable-Driven Robot for Upper and Lower Limbs Rehabilitation," **In:** *Handbook of Research on Advancements in Robotics and Mechatronics* (IGI Global, 2015) pp. 284–315.
[42] A. M. Barbosa, J. C. M. Carvalho and R. S. Goncalves, "Cable-driven lower limb rehabilitation robot," *J. Braz. Soc. Mech. Sci. Eng.* **40**(5), 1–11 (2018).
[43] W. M. Nunes, L. A. O. Rodrigues, L. P. Oliveira, J. F. Ribeiro, J. C. M. Carvalho and R. S. Gonçalves, "Cable-Based Parallel Manipulator for Rehabilitation of Shoulder and Elbow Movements," *2011 IEEE İnternational Conference on Rehabilitation Robotics*, Zurich, Switzerland (2011) pp. 1–6.
[44] K. Homma, O. Fukuda, Y. Nagata and M. Usuba, "Study of a Wire-Driven Leg Rehabilitation System," *2004 IEEE/RSJ International Conference on Intelligent Robots and Systems (IROS),* Sendai, Japan (2004) pp. 1668–1673.
[45] S. S. Adler, D. Beckers and M. Buck, *PNF in Practice: An Illustrated Guide* (Springer, Heidelberg, Germany, 2008).
[46] S. McGee, *Evidence Based Physical Diagnosis e-book* (Elsevier, Philadelphia, PA, 2016).
[47] H. Yu, S. Huang, G. Chen, Y. Pan and Z. Guo, "Human-robot ınteraction control of rehabilitation robots with series elastic actuators," *IEEE Trans. Robot.* **31**(5), 1089–1100 (2015).
[48] B. D. M. Chaparro-Rico, D. Cafolla, M. Ceccarelli and E. Castillo-Castaneda, "Experimental characterization of NURSE, a device for arm motion guidance," *J. Healthcare Eng.* **2018**, 1–15, Hindawi (2018) .
[49] B. D. M. Chaparro-Rico, D. Cafolla, M. Ceccarelli and E. Castillo-Castaneda, "NURSE-2 DoF Device for arm motion guidance: Kinematic, dynamic, and FEM analysis," *Appl. Sci.* **10**(6), 2139 (2020).
[50] B. D. M. Chaparro-Rico, D. Cafolla, E. Castillo-Castaneda and M. Ceccarelli, "Design of arm exercises for rehabilitation assistance," *J. Eng. Res.* **8**(3), 204–218 (2020).
[51] E. Akdoğan, M. E. Aktan, A. T. Koru, M. S. Arslan, M. Atlıhan and B. Kuran, "Hybrid impedance control of a robot manipulator for wrist and forearm rehabilitation: Performance analysis and clinical results," *Mechatronics* **49**, 77–91 (2018).
[52] E. Akdoğan and M. A. Adli, "The design and control of a therapeutic exercise robot for lower limb rehabilitation: Physiotherabot," *Mechatronics* **21**(3), 509–522 (2011).
[53] G. Xu, A. Song, L. Pan, X. Gao, Z. Liang, J. Li and B. Xu, "Clinical experimental research on adaptive robot-aided therapy control methods for upper-limb rehabilitation," *Robotica* **32**(7), 1081–1100 (2014).
[54] M. H. Rahman, M. J. Rahman, O. L. Cristobal, M. Saad, J. P. Kenné and P. S. Archambault," "Development of a whole arm wearable robotic exoskeleton for rehabilitation and to assist upper limb movements," *Robotica* **33**(1), 19–39 (2015).
[55] T. Tsumugiwa, Y. Fuchikami, A. Kamiyoshi, R. Yokogawa and K. Yoshida, "Stability analysis for impedance control of robot for human-robot cooperative task system," *J. Adv. Mech. Des. Syst. Manuf.* **71**(7), 113–121 (2005).
[56] L. Masia, H. I. Krebs, P. Cappa and N. Hogan, "Design, Characterization, and İmpedance Limits of a Hand Robot," *IEEE 10th International Conference on Rehabilitation Robotics* (2007) pp. 1085–1089.
[57] H. I. Krebs, B. T. Volpe, D. Williams, J. Celestino, S. K. Charles, D. Lynch and N. Hogan, "Robot-aided neurorehabilitation: A robot for wrist rehabilitation," *IEEE Trans. Neural Syst. Rehabil. Eng.* **15**(3), 327–335 (2007).
[58] E. L. Oyman and M. S. Arslan, "Impedance-Based Control of a Cable Driven Rehabilitation Robot," *2018 6th International Conference on Control Engineering & Information Technology (CEIT)* (IEEE, 2018) pp. 1–6.

https://doi.org/10.1017/S0263574721000357 Published online by Cambridge University Press

Appendix A

Available exercise types with ROMRES are shown in Fig. A1.

Figure A1. *Types of exercises with ROMRES.*

https://doi.org/10.1017/S0263574721000357 Published online by Cambridge University Press

Appendix B

Table B.1. *Passive exercise values.*

Time (s)	Θ (°)	Ψ_1(rad)	Ψ_2(rad)	T_1(Nm)	T_2(Nm)	F_p(N)	F_{aa}(N)	F_{sa}(N)	H_1(mm)	H_2(mm)
215	66.6	6.8	6.6	0.35	−0.24	0.05	2	−20	530.0	0.0
230	76.5	19.1	16.4	0.41	−0.27	0.03	2	−20	486.0	0.0
245	88.0	34.2	21.8	0.34	−0.26	0.01	2	−20	300.2	200.5
260	99.6	41.7	29.7	0.28	−0.25	−0.02	2	−20	151.7	300.0
275	114.4	51.3	39.5	0.27	−0.24	−0.05	2	−20	150.0	300.0
290	110.7	48.2	33.4	0.23	−0.31	−0.04	−2	20	150.0	300.0
305	98.5	39.3	27.4	0.22	−0.31	−0.02	−2	20	150.0	300.0
320	87.2	31.2	18.9	0.21	−0.29	−0.03	−2	20	293.8	210.7
335	76.3	18.1	14.2	0.20	−0.31	−0.02	−2	20	454.5	0.4
350	65.2	4.1	4.2	0.24	−0.31	0.01	−2	20	530.0	0.0

Table B.2. *Assisted exercise values.*

Time (s)	Θ(°)	Ψ_1(rad)	Ψ_2(rad)	T_1(Nm)	T_2(Nm)	F_p(N)	F_{aa}(N)
365	65.5	6.2	6.1	0.34	−0.24	−0.01	2
370	84.9	29.3	25.7	0.45	−0.30	3.91	2
375	92.1	42.6	29.7	0.35	−0.24	1.92	2
380	115.3	53.2	41.1	0.25	−0.25	0.56	2
385	1189	55.8	43.7	0.23	−0.25	0.54	2
390	117.0	53.6	41.6	0.22	−0.31	0.42	−2
395	112.9	50.7	38.6	0.22	−0.32	0.48	−2
400	104.7	43.1	30.7	0.26	−0.43	−2.92	−2
405	66.3	8.8	6.5	0.21	−0.26	−0.20	−2
410	63.5	3.3	3.2	0.24	−0.33	−0.01	−2

Table B.3. *Spasticity exercise values.*

Time (s)	Θ(°)	F_p(N)	F_{aa}(N)
425	67.7	−0.05	−20
450	86.6	0.20	−20
475	71.8	−21.39	−20
500	89.4	0.03	−20
525	111.4	−0.36	−20
550	105.7	−0.19	20
580	90.9	22.52	20
600	88.5	0.27	20
625	71.2	0.33	20
650	68.0	0.29	20

Cite this article: E. L. Oyman, M. Y. Korkut, C. Yilmaz, Z. Y. Bayraktaroglu and M. S. Arslan (2022). "Design and control of a cable-driven rehabilitation robot for upper and lower limbs", Robotica **40**, 1–37. https://doi.org/10.1017/S0263574721000357